Building and Environment 231 (2023) 110028

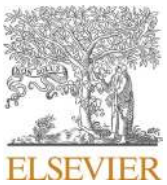

Contents lists available at ScienceDirect

Building and Environment

journal homepage: www.elsevier.com/locate/buildenv

# Numerical method for solving coupled heat and mass transfer through walls for future integration into an urban climate model

Margot Ruiz [a,b,*], Valéry Masson [b], Marion Bonhomme [a], Stéphane Ginestet [a]

[a] LMDC, Université de Toulouse, INSA, UPS, Toulouse, France
[b] CNRM, Université de Toulouse, Météo-France, CNRS, Toulouse, France

ARTICLE INFO

*Keywords:*
Hygrothermal behaviour
Urban climate model
Numerical scheme
Inter-model validation
Wall

ABSTRACT

Numerous studies of hygrothermal transfers through walls have highlighted the impacts of this phenomenon on energy consumption and indoor conditions. However, urban scale models that aim to simulate weather conditions and urban heat island effects within cities neglect moisture transfer through walls. The objective of this paper is to propose a method for solving this phenomenon that could be integrated into an urban climate model. This kind of integration requires the numerical schemes to be adapted as well as the spatiotemporal scales. The proposed method is based on an Implicit/Explicit discretisation scheme and a decoupled numerical approach for solving. Numerical stability is ensured by reducing the time step in critical moments, which are detected by five tests. This method is validated by comparison with a reference model (Delphin ®), on several study cases using different wall compositions and climates. A mesh sensitivity analysis is performed and shows that low permeability walls require a finer mesh than walls made of highly hygroscopic or capillary active materials. Furthermore, the more layers there are in the wall, the finer the mesh size needs to be. This numerical method allowed a balance to be found between computational cost and accuracy level in accordance with the expectations for an urban climate model. The future integration of this method into an urban climate model will make it possible to carry out energy/climate simulations, including the hygrothermal behaviour of walls, and thus to study its impact at urban scale.

## 1. Introduction

### 1.1. Impacts of moisture transfer through walls

Moisture exchange takes place between the urban canyon and the walls. Walls represent a significant share of moisture sinks in the urban mass balance. For example, in a dense, high-rise city, such as Hong Kong, the walls account for 9.55% of the moisture sinks [1].

The simulation of moisture transfers in urban materials allows wetting and drying phenomena to be represented and thus considers the evaporative cooling phenomenon, which has been widely studied as a strategy to mitigate the Urban Heat Island (UHI) phenomenon. However, studies generally focus on evaporation at horizontal surfaces; only a few evaluate the impact of this phenomenon at wall surfaces [2,3]. Although the evaporative cooling potential of the building façades is lower than that of the ground [3], the evaporation phenomenon at wall surfaces contributes to lowering the air temperature in the canyon and improving pedestrian comfort [4]. Indeed, after a rain event, the wet wall dries, the phenomenon of evaporation occurs, which leads to a decrease in the surface temperature of the walls. A decrease in the comfort index UTCI (Universal Thermal Cimate Index) for a pedestrian in the street canyon of up to 2 °C is then observed [2]. The evaporative cooling potential is largely influenced by the climatic variables of the canyon, in particular solar radiation and wind speed [2].

Furthermore, the reduction of energy consumption makes it possible to reduce anthropogenic emissions to the outside environment and therefore constitutes a lever for action to limit the UHI phenomenon [5]. Numerous studies have shown a significant impact of considering moisture transfer on indoor conditions as well as on occupant comfort and therefore on energy consumption. Indeed, moisture in a wall affects its thermal properties, such as thermal conduction and thermal capacity. Thus, the conduction load may be wrongly estimated and the HVAC equipment incorrectly sized [6–9]. Furthermore, highly hygroscopic materials have been studied for their moisture buffering capacity, that is, their ability to reduce fluctuations in indoor relative humidity [10–12]. Thus, neglecting moisture transfer would lead to a poor

* Corresponding author. 135 Avenue de Rangueil, 31400, Toulouse, France.
*E-mail address:* mruiz@insa-toulouse.fr (M. Ruiz).

https://doi.org/10.1016/j.buildenv.2023.110028
Received 13 September 2022; Received in revised form 14 January 2023; Accepted 17 January 2023
Available online 19 January 2023

**Table 1**
Comparison of discretisation and resolution methods for Delphin, TEB and the proposed method.

| | Delphin [23] | TEB [36] | Proposed method |
|---|---|---|---|
| Discretisation scheme | Fully implicit | Fully implicit | Implicit-Explicit (IMEX) |
| Time step | Variable | 5 min | 5 min (lowered to 10 s in critical moments) |
| Mesh | Variable | 5 nodes | Variable |
| Numerical solution method | Newton-Raphson method (iterative and complex) | Lower-Upper (LU) decomposition | Lower-Upper (LU) decomposition |

estimation of indoor conditions, especially on relative humidity, which is a key variable for occupant comfort [13,14]. Variations have also been observed in the indoor air temperature [15] and in the operating temperature [9]. In addition, some studies have shown a reduction in energy consumption related to the installation of hygroscopic materials, of up to 30% depending on the HVAC systems used and the climate studied [16,17]. Thus, the consideration of moisture transfers on an urban scale would allow to better estimate the energy consumption of buildings, to take into account the potential reduction of energy consumption induced by hygroscopic materials and finally to evaluate the impact of these phenomena on the UHI intensity.

### 1.2. Modelling of moisture transfer through walls at different scales

Since the first work on coupled heat and moisture transfer in building materials [18,19], based on the soil models by Refs. [20,21], many models and tools have emerged (see reviews by Ref. [22]), among which Delphin [23], WUFI [18], MATCH [24] and HAM Tools [25] are the most widely used. They differ in the simplifying assumptions made, the driving potentials used, and the discretisation methods and numerical solution methods employed. The main methods are the finite difference method (with, for example, an explicit, implicit or Crank-Nicholson discretisation scheme), the finite volume method, and the finite element method. Berger et al. [26] propose a comparison of several numerical methods for solving coupled transfers.

Then, external couplings between HAM (Heat, Air and Moisture) and BES (Building Energy Simulation) models made it possible to simulate the interactions between the moisture transfers in the walls and the interior conditions [27]. There are also many consolidated tools that rely on internal coupling to simulate entire buildings, including moisture transfer through walls [28], WUFI-Plus, EnergyPlus [29], TRNSYS, IDA ICE [30], BSim [31], ESP-r [32] and HAMFitPlus [33]. These tools allow the impact of moisture transfers on indoor conditions and energy consumption to be assessed. However, their simulation is limited to one building, and they do not simulate the effects of buildings on the urban canyon conditions.

Coupling between CFD (Computational Fluid Dynamics) and HAM exist and they have the advantage of accurately representing the distribution of WDR (Wind-Driven Rain) on the façade [34]. Other models simulate the urban microclimate by coupling three sub-models: CFD for airflow and wind-driven rain, HAM for heat and moisture transport in

**Table 2**
Mesh characteristics for the three tested versions and the reference.

| Mesh version | First mesh size [m] | Stretch factor [−] | Maximum mesh size [m] | Mesh refinement at the interface between two material layers |
|---|---|---|---|---|
| Version 1 | 0.005 | 2 | 0.5 | No |
| Version 2 | 0.0025 | 1.7 | 0.1 | No |
| Version 3 | 0.001 | 1.5 | 0.1 | No |
| Delphin | 0.001 | 1.3 | 0.05 | Yes |

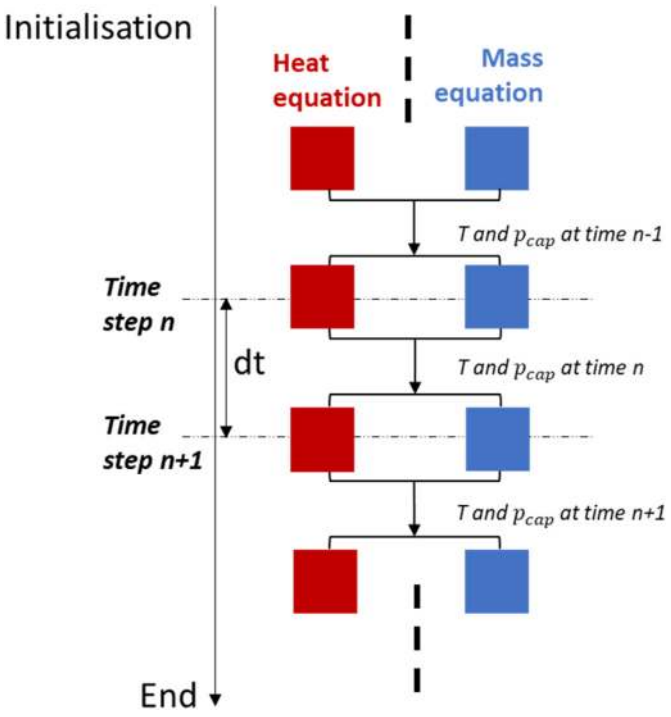


**Fig. 1.** Decoupled numerical approach.

porous media and a radiative model for heat transfer by short- and long-wave radiation [2–4]. These micro-climate models can simulate hydric exchanges between walls and a street canyon. Their main strength is that they take into account the spatial variability along the façade when calculating the CHTC (convective heat transfer coefficient) and CMTC (convective mass transfer coefficient). However, these models consider the interior surface of the wall to be impermeable, which does not allow moisture exchanges between the interior of the building and the street to be simulated. They are not coupled with a model that estimates energy consumption and its effect on climate in the urban canyon. Moreover, urban microclimate models based on CFD have a very high computational cost which does not allow for city-scale simulations over long periods.

On the other hand, a new urban lumped model takes moisture exchanges through wall into account [1]. This model was developed to better understand phenomena related to moisture in urban climates, but it is not designed to accurately forecast hygrothermal conditions.

Another type of model is the Urban Canopy Model (UCM) [35], such as TEB (Town Energy Balance) [36], UCM (Urban Canopy Model) [37] and BEP (Building Effect Parameterization) [38]. These urban climate models are specifically designed to parametrise energy, radiative, hydric and turbulent exchanges between built surfaces and the atmosphere from the neighbourhood to the city scale (which can encompass many grid points representing the neighbourhoods of the agglomeration). They solve balance equations for simplified geometry, (not all individual building shapes can be simulated at the targeted spatial scales), for example using the canyon street concept [39], which means urban areas are represented by an average urban canyon of infinite length. These assumptions allow large areas to be simulated over long periods. These urban climate models do not represent the local urban airflow, which does not allow an accurate estimation of CMTC and CHTC, instead empirical correlations or drag coefficients are used [35]. Similarly, the spatial distribution of the WDR on the façade is not modelled. Some models have the advantage of integrating the assessment of the energy demand of buildings and quantifying interactions between the canyon microclimate and buildings, which is the case of the TEB model including the BEM (Building Energy Model) module [40]. This version

of TEB performs a mass balance to calculate the specific humidity of indoor air considering internal moisture gains, vapour transfers due to window openings, air infiltration or HVAC equipment. A mass balance is also carried out to compute the humidity of the air in the urban canyon taking into account anthropogenic moisture emissions (due to buildings and traffic), moisture exchanges with the atmosphere, vegetation, road and soil. However, the TEB model, like most UCM, neglects mass transfers through walls and consider only heat transfers by conduction.

To the authors' knowledge, no coupling currently exists between UCM and HAM models. Some HAM models propose coupling solutions that could be used to couple hygrothermal transfers in walls with a UCM model. This is the case of Delphin, via Functional Mock-up Interface. However, this type of coupling would have a high computational cost, which would not be suitable for urban scale simulation.

### 1.3. Issues of this study

Current methods for solving coupled mass and heat transfer are not appropriate for the urban scale. Indeed, several adaptations are necessary, particularly in terms of spatiotemporal resolution and the numerical resolution scheme. Moreover, the same level of accuracy is not expected for a wall-scale model and for an urban-scale model since wall-scale models are looking for more and more accurate solutions [41] while urban models are already based on many assumptions. Furthermore, urban scale simulation over long time scales and for entire cities also requires the computational cost to be minimised. There are efficient methods for solving coupled transfers, such as reduction methods [42], but they are not suitable for integration into the numerical scheme of an urban climate model. In addition, current resolution methods are generally based on a variable time step depending on convergence, which makes them complicated to integrate into a fixed time step urban model.

The objective of this paper is to present a new numerical method to facilitate the integration of coupled transfers through walls in an urban climate model. The numerical model of coupled transfers usually consists of two conservation equations (one for energy, the other for mass). In this work, widely used equations will be employed and adaptations will be made only in their numerical solution method. The reliability of the proposed method is verified using boundary conditions representative of an urban environment. The integration of this method into an urban climate model is not carried out in this paper.

Firstly, this paper will present the coupled transfer model used. Then, it will propose an adaptation of the numerical method suitable for future use at the urban scale. It will be validated by confrontation with the results of a reference model (Delphin 6.1.2) on several case studies. Finally, the novelty and originality of this model will be discussed.

## 2. Heat and mass transfer model

Currently, most urban climate models consider heat transfers by conduction through walls but neglect hydric transfers. One equation is solved to describe heat balance in a multilayer wall in 1D:

$$c_{mat}\rho_{mat}\frac{\partial T}{\partial t}=\frac{\partial}{\partial x}\left(\lambda\frac{\partial T}{\partial x}\right) \tag{1}$$

with $c_{mat}$ the heat capacity of the material ($J.kg^{-1}.K^{-1}$), $\rho_{mat}$ the mass density of materials ($kg.m^{-3}$), $\lambda$ the thermal conductivity ($W.m^{-1}.K^{-1}$), and $T$ the temperature (K).

This equation refers to heat storage and transfer for a unit volume.

Thermal properties vary spatially according to the material layer. However, these models do not consider the variation of thermal properties over time as a function of the wall conditions. For example, the effect of water content on thermal properties is neglected.

This section presents a widely used model for considering coupled mass and heat transfer, and thus the impact of moisture exchange on heat transfer.

### 2.1. Hypothesis

The model presented describes heat and mass transfer in a multilayer wall. This model includes not only the heat transfer by conduction but also the effect of each layer's water content on the thermal properties and its contribution to heat storage. It also solves vapour and liquid water transfer through wall and the heat transfer induced by these water transports is considered. Finally, consideration of all these phenomena will make it possible to describe the thermal and hydric fluxes through the wall and exchanges with its environments.

This model represents hygrothermal transfer in 1D, which does not enable vertical and punctual phenomena, such as thermal bridges, to be modelled. The model is also based on several usual assumptions that the following phenomena can be neglected [43].

- Vapour diffusion under temperature gradients (Soret effect),
- Effect of gravity in pores,

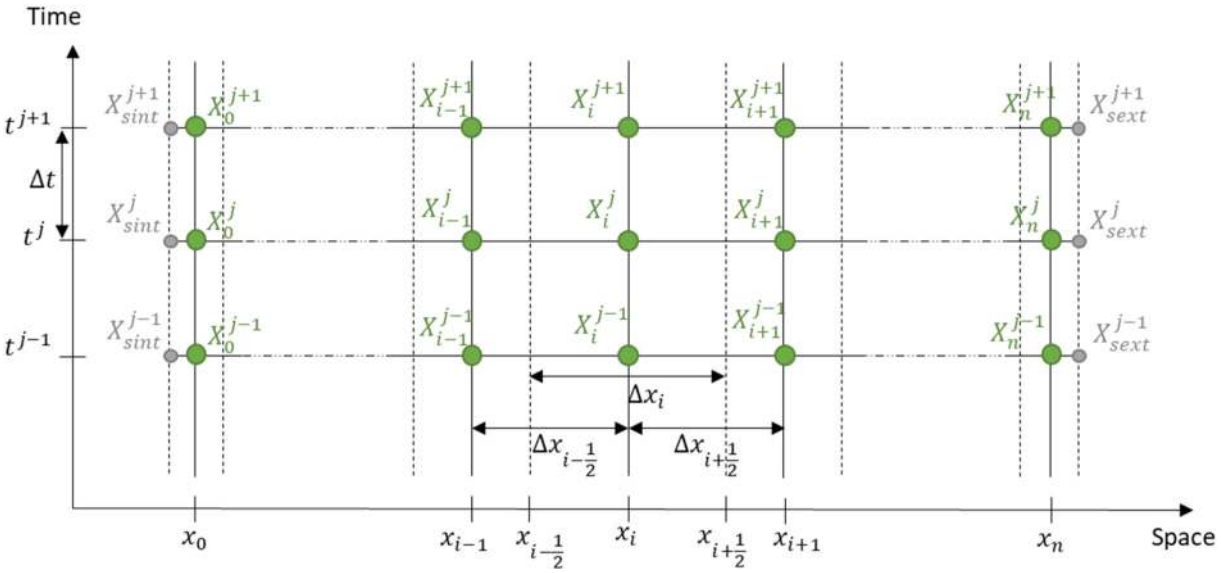


**Fig. 2.** Spatiotemporal discretisation grid for an unknown variable X.

- Influence of temperature on moisture storage,
- Contribution of gas phases to heat storage,
- Air transfer through the wall.

Also, ice formation, pore weathering processes and chemical reactions are not modelled, as the impact of these phenomena on coupled transfers is considered low [18].

The hysteresis effect between the adsorption and desorption curves is complex to model and is often neglected by hygrothermal models [44]. A study compared the results of simulations using the adsorption curve, the desorption curve or taking into account hysteresis and showed little difference between the three versions [45]. Although more recent work has shown that the phenomenon of hysteresis can have a significant impact in certain cases [46], the choice was made to neglect this phenomenon, in particular because a high level of accuracy is not expected at the targeted simulation scale. In this work, the desorption curve is used to describe the moisture storage, which is also the assumption made in Delphin [47].

### 2.2. Governing equations

The model is based on the work of [23] and consists of two equations (1) and (2), corresponding to the energy and mass conservation balances respectively. The left-hand side corresponds to storage terms and the right-hand side represents transport terms. Several types of transfer are considered: heat transfer by conduction, transfer of water in vapour form using Fick's diffusion, and transfer of water in liquid form based on Darcy's law.

$$\frac{\partial u}{\partial t} = \frac{\partial}{\partial x}\left(\lambda \frac{\partial T}{\partial x} + h_l K_l \frac{\partial p_c}{\partial x} + h_v K_v \frac{\partial p_v}{\partial x}\right) \tag{2}$$

$$\frac{\partial \rho^{v+w}}{\partial t} = \frac{\partial}{\partial x}\left(K_l \frac{\partial p_c}{\partial x} + K_v \frac{\partial p_v}{\partial x}\right) \tag{3}$$

$$h_l = c_l\left(T - T_{ref}\right) \tag{4}$$

$$h_v = c_v\left(T - T_{ref}\right) + L_v \tag{5}$$

with $u$ the energy density ($J.m^{-3}$), $\rho^{v+w}$ the mass density of water in liquid and vapour form ($kg.m^{-3}$), $h_l$ the liquid water enthalpy (J), $h_v$ the vapour enthalpy (J), $K_l$ the liquid conductivity (s), $p_c$ the capillary pressure (Pa), $p_v$ the vapour pressure (Pa), $K_v$ the vapour permeability of the material ($kg.m^{-1}.s^{-1}.Pa^{-1}$), $c_l$ the heat capacity of liquid water (J/K), $c_v$ the heat capacity of water vapour (J/K), $T_{ref}$ the reference temperature (K) and $L_v$ the heat of vaporization (2500 $J.kg^{-1}$).

In agreement with the assumptions made, the storage terms are written as follows:

$$\frac{\partial u}{\partial t} = \frac{\partial}{\partial t}\left(\rho_{mat} c_{mat} T + w c_l\left(T - T_{ref}\right)\right) \tag{6}$$

$$\frac{\partial \rho^{v+w}}{\partial t} = \frac{\partial w}{\partial t} \tag{7}$$

with $w$ the water content ($kg.m^{-3}$),

The equations thus written include three driving potentials: temperature, vapour pressure and capillary pressure. However, only two equations are solved, so the number of unknown variables must be reduced to two. The driving potential selected for moisture is the capillary pressure. The capillary pressure is the driving potential linked to Darcy's law and is used in HAM-BE [48], Delphin [23] and also in the model presented in this paper [43]. When compared to benchmark simulations by Ref. [49], it gives very satisfactory numerical results. To express the two previous equations as a function of the two driving potentials chosen (temperature and capillary pressure), the Kelvin relation is used, and the following equations are obtained:

$$\left(c_{mat}\rho_{mat} + c_l\, w\right)\frac{\partial T}{\partial t} + \left(c_l\left(T - T_{ref}\right)\right)\frac{\partial w}{\partial p_c}\frac{\partial p_c}{\partial t} =$$

$$\frac{\partial}{\partial x}\left(\left(\lambda + h_v K_v\left[\frac{\partial p_{v,sat}}{\partial T}\varphi + \frac{p_c}{T}\frac{\rho_v}{\rho_l}\right]\right)\frac{\partial T}{\partial x} + \left[h_l K_l + h_v K_v \frac{\rho_v}{\rho_l}\right]\frac{\partial p_c}{\partial x}\right) \tag{8}$$

$$\frac{\partial w}{\partial p_c}\frac{\partial p_c}{\partial t} = \frac{\partial}{\partial x}\left(K_v\left[\frac{\partial p_{v,sat}}{\partial T}\varphi + \frac{p_c}{T}\frac{\rho_v}{\rho_l}\right]\frac{\partial T}{\partial x} + \left[K_l + K_v\frac{\rho_v}{\rho_l}\right]\frac{\partial p_c}{\partial x}\right) \tag{9}$$

### 2.3. Boundary conditions

The wall is the interface between the indoor environment and the outdoor conditions. It is therefore subject to different stresses on its two sides.

At the exterior surface, the wall is exposed to changing weather conditions such as temperature, relative humidity, rain, solar radiation and long-wave radiation from the atmosphere and other surfaces of the urban environment. This leads to heat ($q_{sext}$) and water ($j_{sext}$) fluxes, decomposed as:

$$q_{sext} = q_{conv} + q_{SW,abs} + q_{LW,net} + h_v j_{conv} + h_l\, j_{rain} \tag{10}$$

$$j_{sext} = j_{conv} + j_{rain} \tag{11}$$

with $q_{conv}$ the convective heat flux ($W.m^{-2}$), $j_{conv}$ the convective mass flux ($kg.m^{-2}.s^{-1}$), $q_{SW,abs}$ the short-wave radiation flux absorbed by the façade ($W.m^{-2}$), $q_{LW,net}$ the net long-wave radiation flux exchanged between the wall and its surroundings ($W.m^{-2}$), and $j_{rain}$ the wind-driven rain flow incident on the façade ($kg.m^{-2}.s^{-1}$).

On the interior side, the boundary conditions for heat and mass equations are restricted to convective heat and mass exchange.

$$q_{sint} = q_{conv} + h_v j_{conv} \tag{12}$$

$$j_{sint} = j_{conv} \tag{13}$$

By rewriting the boundary conditions as a function of the two driving potentials, the following equations are obtained:

$$q_{sext} = h_{conv,th}\left(T_{ext} - T_{sext}\right) + \alpha q_{SW,inc} + \varepsilon\sigma\left(T_{equiv}^4 - T_{sext}^4\right)$$

$$+L_v h_{conv,m}\left[p_{v,ext} - p_{sat}(T_{sext})exp\left(\frac{p_{c,sext}}{\rho_l R_v T_{sext}}\right)\right] + c_l\left(T_{ext} - T_{ref}\right)j_{rain} \tag{14}$$

$$j_{sext} = h_{conv,m}\left[p_{v,ext} - p_{sat}(T_{sext})exp\left(\frac{p_{c,sext}}{\rho_l R_v T_{sext}}\right)\right] + j_{rain} \tag{15}$$

$$q_{sint} = h_{conv,th}(T_{int} - T_{sint}) + L_v h_{conv,m}\left[p_{v,int} - p_{sat}(T_{sint})exp\left(\frac{p_{c,sint}}{\rho_l R_v T_{sint}}\right)\right] \tag{16}$$

$$j_{sint} = h_{conv,m}\left[p_{v,int} - p_{sat}(T_{sint})exp\left(\frac{p_{c,sint}}{\rho_l R_v T_{sint}}\right)\right] \tag{17}$$

with $h_{conv,th}$ the convective heat coefficient ($W.m^{-2}.K^{-1}$), $h_{conv,m}$ the convective mass coefficient ($kg.m^{-2}.s^{-1}.Pa^{-1}$), $\alpha$ the absorption coefficient, $q_{SW,inc}$ the incident short-wave radiative flux ($W.m^{-2}$) and $\varepsilon$ the emissivity of the façade.

## 3. Numerical method

This section focuses on a numerical scheme that is proposed to solve coupled transfers and would be suitable for integration into an urban climate model. The proposed numerical scheme must correspond to an urban model scheme and operate over large spatiotemporal scales. Compromises between accuracy and computation time must be found, knowing that simulations at the city scale are based on many assumptions.

### 3.1. Discretisation scheme

The equation of coupled transfers has resulted in a system of non-linear partial differential equations to be solved on a continuous domain. The discretisation of equations leads to a system of linear equations on a discrete domain, which can be solved more simply.

The comparison of the discretisation and resolution methods of two reference models (Delphin for wall scale and TEB for urban scale) (Table 1) shows strong differences, concerning the time step, mesh size and numerical method. Firstly, the time steps and mesh sizes are variable and fine in Delphin whereas, in TEB they are considered constant and very coarse. Furthermore, the resolution in Delphin is based on a complex, iterative method, which involves performing iterations at each time step until convergence is reached.

Thus, in order to match the numerical schemes of an urban climate model, the proposed numerical scheme performs the discretisation based on the finite difference method. Regarding the discretisation scheme, explicit schemes are not suitable for the integration of coupled transfers to urban model like TEB but fully implicit schemes must be associated with iterative methods to be stable. It is not possible to integrate this type of resolution method into an urban climate model. Finally, an Implicit-Explicit (IMEX) scheme imposes itself, as it allows sub-iterations to be avoided and is numerically stable and consistent [50]. This semi-implicit scheme has been used in several studies and the accuracy of the results obtained was satisfactory in all these cases [41, 51,52]. A comparison with a fully implicit scheme even showed that the IMEX scheme had a lower computation time and provided more accurate results than an implicit scheme [50]. In these two discretisation schemes, the scheme considered for solving the field is implicit, since the unknown variables are calculated at time step j+1. The difference between a fully implicit scheme and an IMEX scheme is based on the calculation of the non-linear properties at each time step. Indeed, for the implicit scheme, the storage and diffusivity coefficients are calculated at time step j+1, while in the IMEX scheme, they are calculated at time step j, which avoids sub-iterations. Furthermore, the temporal discretisation is done by first-order backward finite differences and the spatial discretisation consists of approximating by a second-order central difference.

Concerning the spatial discretisation, three mesh versions were tested for the proposed method. Table 2 describes the characteristics of these versions and of the mesh chosen for the simulations carried out with Delphin.

### 3.2. Decoupled numerical approach

These equations (8) and (9) can be written as a matrix system. This system is solved by applying the lower-upper (LU) decomposition method. The heat and mass equations are solved through a decoupled numerical approach, which consists of solving two separate matrix systems, one for moisture and one for heat, at each time step (Fig. 1).

However, temperature is involved in the mass equation and therefore is not considered as an unknown in this equation but is set equal to its values at the previous time step. A similar approach is used for capillary pressure in the heat equation. The following discretised equations are then obtained, for solving at time step j+1 and at node i (Fig. 2).

$$0=(C_{TT})_i^j\frac{T_i^{j+1}-T_i^j}{\Delta t}+(C_{TP})_i^j\frac{p_{c,i}^j-p_{c,i}^{j-1}}{\Delta t}+\left[\frac{(K_{TT})_{i-1/2}^j}{\Delta x_i}\frac{(T_i^{j+1}-T_{i-1}^{j+1})}{\Delta x_{i-1/2}}-\frac{(K_{TT})_{i+1/2}^j}{\Delta x_i}\frac{(T_{i+1}^{j+1}-T_i^{j+1})}{\Delta x_{i+1/2}}\right]+\left[\frac{(K_{TP})_{i-1/2}^j}{\Delta x_i}\frac{(p_{c,i}^j-p_{c,i-1}^j)}{\Delta x_{i-1/2}}-\frac{(K_{TP})_{i+1/2}^j}{\Delta x_i}\frac{(p_{c,i+1}^j-p_{c,i}^j)}{\Delta x_{i+1/2}}\right] \tag{18}$$

$$0=(C_{PT})_i^j\frac{T_i^j-T_i^{j-1}}{\Delta t}+(C_{PP})_i^j\frac{p_{c,i}^{j+1}-p_{c,i}^j}{\Delta t}+\left[\frac{(K_{PT})_{i-1/2}^j}{\Delta x_i}\frac{(T_i^j-T_{i-1}^j)}{\Delta x_{i-1/2}}-\frac{(K_{PT})_{i+1/2}^j}{\Delta x_i}\frac{(T_{i+1}^j-T_i^j)}{\Delta x_{i+1/2}}\right]+\left[\frac{(K_{PP})_{i-1/2}^j}{\Delta x_i}\frac{(p_{c,i}^{j+1}-p_{c,i-1}^{j+1})}{\Delta x_{i-1/2}}-\frac{(K_{PP})_{i+1/2}^j}{\Delta x_i}\frac{(p_{c,i+1}^{j+1}-p_{c,i}^{j+1})}{\Delta x_{i+1/2}}\right] \tag{19}$$

The coefficients of the matrices are written as follows:

$$C_{TT}=c_{mat}\rho_{mat}+c_l\,w;$$
$$C_{TP}=c_l(T-T_{ref})\frac{dw}{dp_c};$$
$$C_{PP}=\frac{dw}{dp_c};$$
$$C_{PT}=0;$$
$$K_{TT}=\lambda+L_vK_{PT};$$
$$K_{TP}=c_l(T-T_{ref})K_l+L_vK_v\frac{p_v}{R_vT\rho_l};$$
$$K_{PP}=K_l+K_v\frac{p_v}{R_vT\rho_l}$$
$$\text{and } K_{PT}=K_v\frac{p_v}{R_vT^2}\left(L_v-\frac{p_c}{\rho_l}\right)$$

The coefficients $C_{**}$ and $K_{**}$ also depend on the temperature and capillary pressure, two variables whose values are still unknown at time step j+1. Their calculation is based on the values obtained at time step j.

Spatial discretisation implies calculating the value of some quantities between two points of the mesh. The method applied for this calculation is the following: $\Delta x_{i-1/2}=(\Delta x_i+\Delta x_{i-1})/2$;

$$\Delta x_{i+1/2}=(\Delta x_i+\Delta x_{i+1})/2;$$
$$K_{**i-1/2}=(K_{**i}+K_{**i-1})/2$$
$$\text{and } K_{**i+1/2}=(K_{**i}+K_{**i+1})/2$$

The discretisation of the boundary conditions is performed as follows:

$$q_{sext}^{j+1}=h_{conv,th}\left(T_{ext}^{j+1}-T_{sext}^{j+1}\right)+L_vh_{conv,m}\left(p_{v,ext}^{j+1}-p_{v,sext}^{j}\right)+j_{rain}c_l\left(T_{ext}^{j+1}-T_{ref}\right)+\alpha q_{CLO,inc}+\varepsilon\sigma\left(\frac{T_{equiv}^{j+1}-T_{sext}^{j}}{2}\right)^3\left(T_{equiv}^{j+1}-T_{sext}^{j+1}\right) \tag{20}$$

$$j_{sext}^{j+1}=h_{conv,m}\left(p_{v,ext}^{j+1}-p_{v,sext}^{j}\left(1+\frac{1}{\rho_lR_vT_{sext}^{j}}\left(p_{c,sext}^{j+1}-p_{c,sext}^{j}\right)\right)\right)+j_{rain} \tag{21}$$

$$q_{sint}^{j+1}=h_{conv,th}\left(T_{int}^{j+1}-T_{sint}^{j+1}\right)+L_vh_{conv,m}\left(p_{v,int}^{j+1}-p_{v,sint}^{j}\right) \tag{22}$$

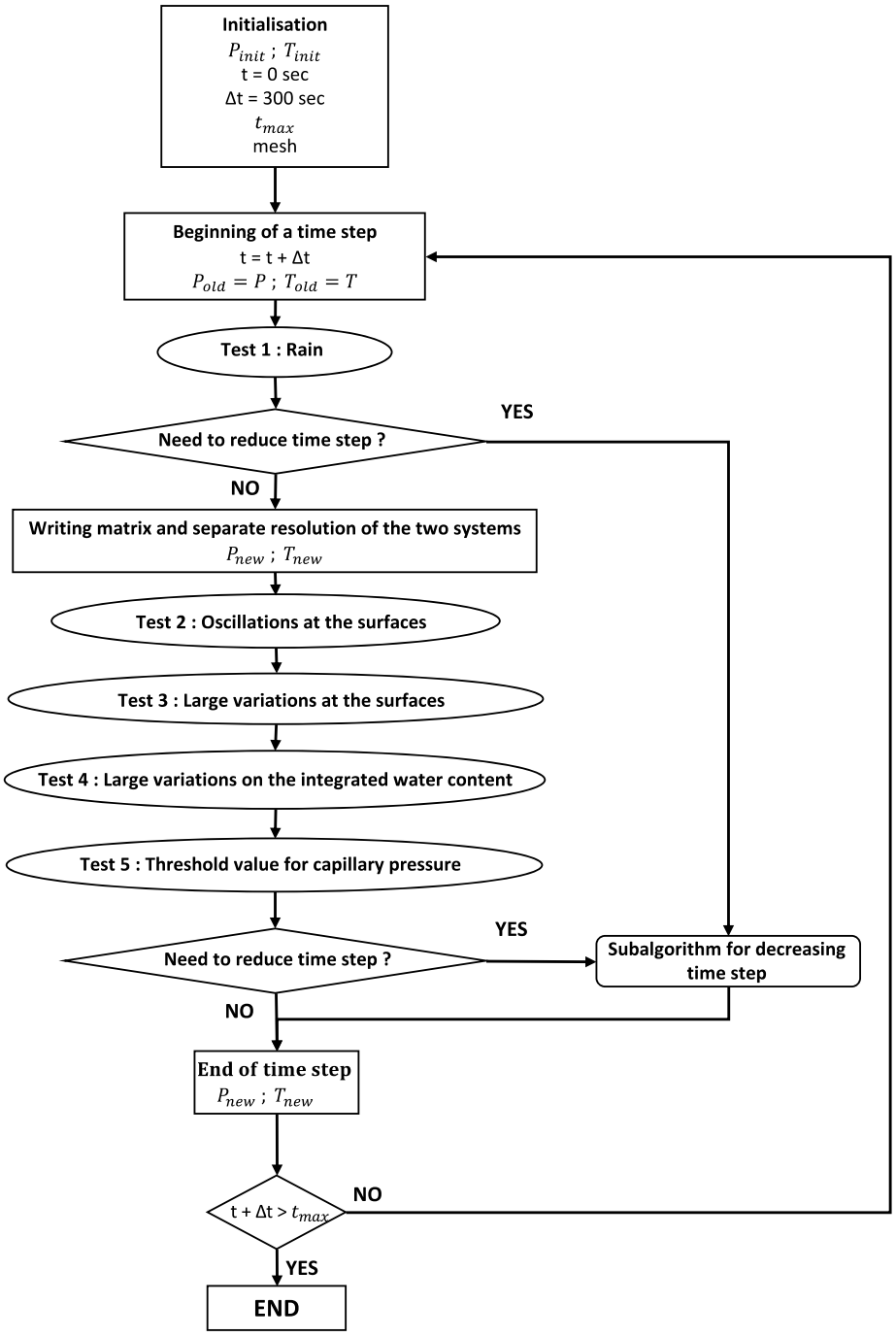


**Fig. 3.** Algorithm of the proposed numerical method.

$$j_{sint}^{j+1} = h_{conv,m}\left(p_{v,int}^{j+1} - p_{v,sint}^{j}\left(1 + \frac{1}{\rho_l R_v T_{sint}^{j}}\left(p_{c,sint}^{j+1} - p_{c,sint}^{j}\right)\right)\right) \quad (23)$$

The variables at the surfaces are approximated by their value at the nearest node.

### 3.3. Numerical stability

To ensure numerical stability, the time step (usually 5 min) is reduced to 10 s at the most critical moments. To identify critical moments for convergence, five tests are performed (Fig. 3).

The first test checks the amount of rain absorbed by the wall. Thus, when the rain flux absorbed is higher than the threshold value, the time step is decreased for both equations (heat and mass).

The second test detects oscillations on temperatures or capillary pressures simulated on the internal and external surfaces. The test is performed only if the recorded difference between the current time step and the previous time step is higher than a certain threshold value. Then, it checks the sign of the last two variation rates. If an increase is followed by a decrease or vice versa, there are oscillations and the time step is decreased for the equation(s) concerned, i.e., if an oscillation occurs in capillary pressure on at least one surface, the time step is decreased for the mass equation and if an oscillation is detected for temperature, the time step of the heat equation is decreased. The time step can therefore be decreased for one equation or for both equations simultaneously. Fig. 4 shows the procedure of this test for capillary pressure at the

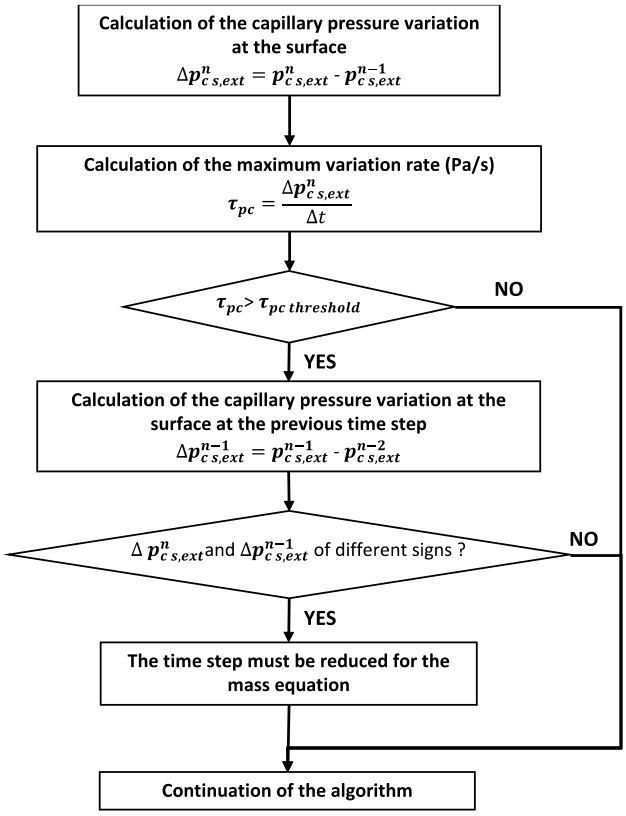


**Fig. 4.** Algorithm of Test 2 for capillary pressure at the exterior surface.

exterior surface. The same test is performed for the interior surface and also for the temperature at the interior and exterior surfaces.

The third test checks that the variation rate in absolute value is lower than a threshold value fixed for the temperature and that for the capillary pressure. If the criterion is not respected for capillary pressure on at least one of the two surfaces at this time step, there is a decrease for the mass equation – and idem for temperature with the heat equation.

The fourth test calculates the integrated water content of the wall and then its variation rate from the current time step to the next. If this rate exceeds a certain threshold, the time step is decreased for the mass conservation equation.

Finally, the last test ensures that capillary pressure does not become positive, as this is impossible from a physical point of view. If the capillary pressure at a mesh point exceeds a threshold value, the time step of the mass equation must be decreased. If decreasing the time step is not sufficient to solve the problem, the capillary pressure is replaced by a threshold value.

Table 3 summarises all the threshold values used in each test. These values were chosen to represent acceptable thresholds, but also to obtain results with satisfactory accuracy and limited computational cost.

**Table 3**
Threshold values for the five tests.

| Test number | Variable | Units | Threshold values |
|---|---|---|---|
| Test 1 | Absorbed rain rate | $kg.m^{-2}.s^{-1}$ | 0.00002 |
| Test 2 | Variation rate for | | |
| | - Capillary pressure | $Pa.min^{-1}$ | 40000 |
| | - Temperature | $°C.min^{-1}$ | 0.05 |
| Test 3 | Variation rate for | | |
| | - Capillary pressure | $Pa.min^{-1}$ | 400000 |
| | - Temperature | $°C.min^{-1}$ | 0.6 |
| Test 4 | Variation rate for integrated water content | $kg.m^{-3}.min^{-1}$ | 0.01 |
| Test 5 | Capillary pressure limit | $Pa$ | 0 |
| | Replacement value for capillary pressure | $Pa$ | −1000 for mesh versions 1 and 2 and -1e6 for mesh version 3 |

## 4. Validation by inter-model comparison

Three main methods exist for the validation of a hygrothermal model: experimental validation, theoretical validation based on an analytical solution, and validation by inter-model comparison [53]. This paper uses the last method to validate the proposed numerical method. The comparison is carried out on results simulated with the reference model Delphin (version 6.1.2), which has been widely validated and is frequently used [54].

### 4.1. Assessment method

Model evaluation focuses on the verification of data used to calculate convective exchanges with the indoor environment and outdoor urban environment as well as the overall consistency of the simulated data inside the wall. Thus, six variables are chosen to evaluate the model: temperature and vapour pressure at the interior surface, temperature and vapour pressure at the exterior surface, average temperature in the wall, and water content integrated over the whole wall. To verify the temporal evolution of these six variables, the results simulated are compared with those from Delphin. The error (absolute or relative) due to our method is then estimated at each time step with respect to this reference:

$$err^{j}_{abs} = \left| X^{j}_{method} - X^{j}_{Delphin} \right| \tag{24}$$

$$err^{j}_{rel} = \left| \frac{X^{j}_{method} - X^{j}_{Delphin}}{X^{j}_{Delphin}} \right| \tag{25}$$

with $X^{j}_{method}$ the value of the variable calculated by the proposed method at time step j, and $X^{j}_{Delphin}$ the value of the variable calculated by Delphin at time step j.

### 4.2. Cases studied

The validation method is based on the simulation of a classical configuration presented in Fig. 5. A wall, for which the initial conditions are defined, is subjected to constant indoor conditions and to outdoor conditions calculated from a weather file.

#### 4.2.1. Calculation of urban boundary conditions

This section presents the methods used to obtain boundary conditions representative of an urban environment. The same boundary conditions are used as inputs for Delphin and the proposed method.

The calculation of boundary conditions at the exterior surface from the weather files depends on the urban form studied. In this work, the urban environment chosen to carry out these calculations was the medieval district of Cahors, a small town in the south-west of France (44°26′54″N 1°26′29″E). This neighbourhood corresponds to a dense city centre with narrow streets. The wall studied is located on the first floor of a east-facing façade.

*4.2.1.1. Convective coefficient.* CHTC and CMTC are essential variables for assessing heat and mass exchange at urban surfaces. Many formulations exist to calculate CHTC [55–57], these are generally based on empirical formulae that depend on the local wind speed and the temperature difference between the surface and the air. It is difficult to conclude which is the most appropriate method to use [56]. In this work, the formulation employed is the DOE-2 model [58]. The convection

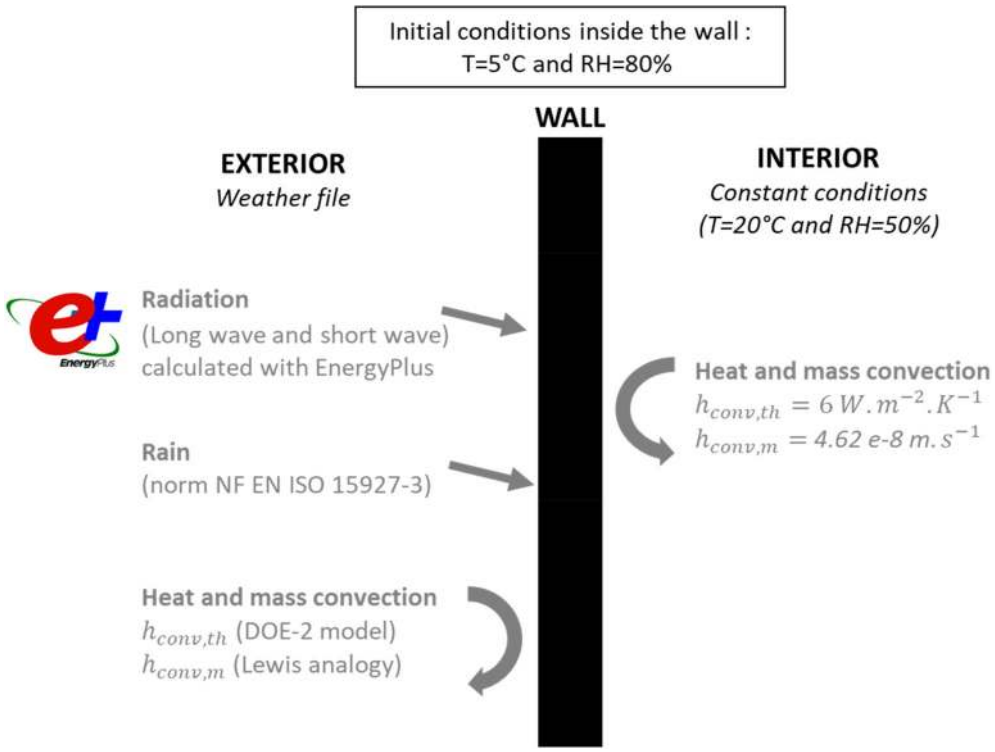


**Fig. 5.** Schematic representation of the simulated configuration.

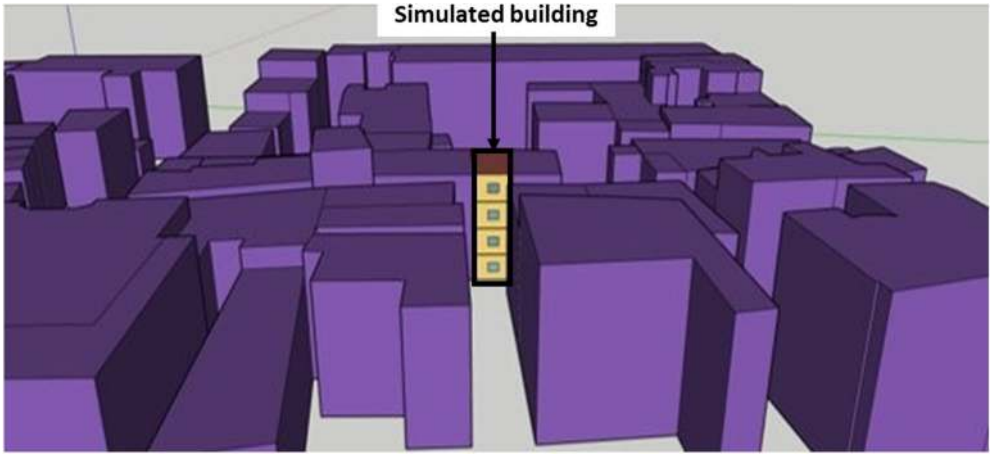


**Fig. 6.** Urban area simulated in Energy Plus to define the boundary conditions, with a view of the east-facing building considered to test the model.

coefficients are input data in both tools compared. They are computed beforehand in EnergyPlus, using DOE-2 model. The output variable for CHTC is called "Surface Outside Face Convection Heat Transfer Coefficient [W/m2-K](Hourly)" in the EnergyPlus tool.

The CMTC is calculated from the value of the CHTC, applying the Lewis analogy [43]:

$$h_{conv,m} = 7.7 * 10^{-9}\ h_{conv,th} \tag{26}$$

*4.2.1.2. Short-wave radiation.* Short-wave radiation incident on the vertical wall were calculated using the EnergyPlus software. This software takes into account the three components of solar radiation: direct, diffuse and reflected. It performs an energy simulation for a single building of interest (Fig. 6). The other buildings are considered as solar masks and are used in the calculation of the inter-reflection of solar radiation between the external surfaces (using the ray-tracing method). The advantage of the EnergyPlus software is that it allows to consider a complex urban morphology.

Thus, the short-wave radiative flux incident on the first-floor wall is calculated using EnergyPlus, which takes into account the urban environment. The boundary condition required to describe incident solar radiation in the hygrothermal model is provided by the output variable called "Surface Outside Face Incident Solar Radiation Rate per Area [W/m2](Hourly)" in the EnergyPlus nomenclature. The solar radiation flux absorbed by the wall is computed from incident solar radiation flux by multiplying by solar absorptance coefficient (fixed at 0.7 for all the façades in this study).

*4.2.1.3. Long-wave radiation.* The default mode of EnergyPlus, calculates the longwave radiative flux by assuming that the building exchanges only with the ground, the sky and an environment whose temperature is estimated to be equal to that of the air. Thus, in the

default mode, radiative exchanges between buildings are not modelled. A multi-building co-simulation strategy was developed to quantify the infrared exchanges between buildings. The first step is to calculate the view factors between the surfaces of the studied building and those of the surrounding buildings. Then, this method consists of simulating several buildings separately with EnergyPlus, using the view factors and the surface temperatures of the surrounding buildings as input data to calculate the long-wave radiation. Several iterations are carried out: in each iteration, all buildings are simulated over the whole simulated period (one year) and the long-wave radiation is computed from the surface temperatures of the other buildings calculated in the previous iteration. Iterations are performed until convergence on the surface temperatures of the building of interest is reached. The long-wave radiation calculated for the studied facade is then used as input in the two tools being compared. In this study, this boundary condition is derived from the output variable "Surface Outside Face Net Thermal Radiation Heat Gain Rate per Area [W/m2](Hourly)", computed by EnergyPlus for the first-floor wall of the east-facing façade.

*4.2.1.4. WDR.* The calculation of the WDR in the developed method is done by applying the method used in the Delphin tool, in order to obtain easily comparable results. The incident rainfall was thus calculated from weather data, using the WDR model of ISO 15927-3 [59]. This norm gives the following equation to quantify the WDR exposure I in an hour [60]:

$$I = \frac{2}{9} v r^{8/9} \cos(D - \theta) \tag{27}$$

With $v$ the average hourly wind speed ($m.s^{-1}$), r the hourly precipitation (mm), D the hourly mean wind direction (°), $\theta$ the wall direction (°).

This semi-empirical formula ignores the effect of geometry, obstacles, and topography on WDR rain exposure of a façade. To take these elements into account, an attenuation coefficient is calculated from the following four factors: a factor for terrain variations ($C_R$), a factor for topography ($C_T$), an obstacle factor (O) and a wall factor (W.)

$$Iw = C_R * C_T * O * W * I \tag{28}$$

In the urban environment studied, the product of these four coefficients is fixed at 0.07.

The rain flux incident on the wall $j_{imp}$ is estimated from the WDR exposure of the wall in an hour $Iw$. However, not all the incident flux can be systematically absorbed by the wall, it depends on the moisture conditions in the wall. The maximal absorbed rain flux is calculated from the following equation:

$$j_{max} = -\left(K_l(w_{sat}), K_l\left(w^{elem}\right)\right).\frac{p_c^{elem}}{x^{elem}} \tag{29}$$

With $j_{max}$ the maximum water flow into the boundary element ($kg.m^{-2}.s^{-1}$), $w_{sat}$ the saturation water content of material ($kg.m^{-3}$), $w^{elem}$ the current water content in boundary element($kg.m^{-3}$), $p_c^{elem}$ the capillary pressure in boundary element (Pa) and thickness of boundary element (m).

The real absorbed flux is then deduced by taking the minimum value between the normal rain flux at the façade and the maximum flux:

$$j_{rain} = \min\left(j_{imp}, j_{max}\right) \tag{30}$$

With $j_{imp}$ the water flow normal to the surface ($kg.m^{-2}.s^{-1}$).

### 4.2.2. Wall configuration

The evaluation was carried out on fifteen walls (Table 4) whose composition differed by the number of layers and the properties of the materials. Thus, the tool was tested for traditional or more modern walls, possibly combined with internal or external insulation systems: impermeable, hygroscopic or capillary active.

**Table 4**
Details of the composition of the walls studied.

| N° | Composition of the walls from the outside to the inside |
|---|---|
| 1 | Brick (0.4 m) – Hemp and lime insulation (0.1 m) |
| 2 | Hemp and lime insulation (0.1 m) – Brick (0.4 m) |
| 3 | Brick (0.4 m) |
| 4 | Hemp and lime insulation (0.1 m) |
| 5 | Brick (0.4 m) – Calcium silicate (0.1 m) |
| 6 | Brick (0.4 m) – Mineral wool (0.1 m) – Vapour retarder (0.001 m) – Gypsum board (0.01 m) |
| 7 | Lime plaster (0.001 m) – Mineral wool (0.1 m) – Brick (0.4 m) |
| 8 | Raw earth (0.2 m) |
| 9 | Concrete (0.2 m) |
| 10 | Mineral fine plaster (0.015 m) – Expanded polystyrene (0.1 m) – Concrete (0.2 m) |
| 11 | Concrete (0.2 m) – Mineral wool (0.1 m) – Vapour retarder (0.001 m) – Gypsum board (0.01 m) |
| 12 | Old brick (0.215 m) |
| 13 | Old brick (0.215 m) – Perforated composite foil (0.001 m) – Phenolic foam (0.05 m) – Composite foil (0.001 m) – Plasterboard (0.0125 m) |
| 14 | Old brick (0.215 m) – Glue mortar (0.0065 m) – Calcium silicate (0.14 m) – Lime plaster (0.004 m) |
| 15 | Old brick (0.215 m) – Mineral fine plaster (0.008 m) – Wood fibre board (0.1 m) – Gypsum board (0.012 m) |

The properties of all materials are described in Table 5. The characteristics of raw earth were taken from the paper of [61] and those of the brick and the lime-hemp were the results of the characterisation of the materials from the living-lab located in Cahors [62]. Properties of other materials were extracted from the Delphin database. The compositions of the complex historical walls (from n°12 to n°15) were taken from the work of [63].

All the walls presented in Table 4 were simulated in the climate of Cahors, using the 2016 weather file of the station located at the Le Montat aerodrome near Cahors. The numerical method was also assessed in more extreme climates, to test its limits. Walls 1 and 10 were evaluated in two additional climates: the desert climate (hot and dry) of Aswan (Egypt) and the tropical climate (hot and humid) of Manaus (Brazil). The weather files used to describe the climate of Aswan and Manaus were taken from the EnergyPlus database. The indoor conditions were considered constant at a temperature of 20 °C and a relative humidity of 50% in all cases.

## 4.3. Mesh sensitivity analysis

The objective of this section was to find a compromise for the spatial discretisation, as urban climate models currently solve heat transfers in wall with few nodes and coupled transfer tools generally use finer meshes. Moreover, it is recommended to apply a smaller mesh size near surfaces and at the interface between different material layers, since these areas are generally subject to larger variations than the centre of the materials.

Several meshes were tested, differing in the size of the first mesh, the rate of increase, and the number of nodes. The three versions studied did not include any mesh refinement at the interface between two material layers (Table 2).

The simulations for each wall and for the different climates were run over a full year with the three mesh versions. The difference between the results of the proposed scheme and those of Delphin was evaluated at each time step. In order to present the results in a concise way, the time during which the difference exceeded a certain threshold value (Table 6) was calculated. The results of a simulation were considered unsatisfactory when the difference exceeded the threshold value more than 10% of the time for at least one of the six variables (i.e. when a red box is present on a line of Figs. 6–8).

The first mesh version consisted of a first mesh of 5 mm and a stretch factor of 2. The proposed scheme generally worked well for walls composed of one or two layers of materials and efficiently simulated

**Table 5**
Material properties used for the simulation.

| | Density | Thermal capacity | Dry thermal conductivity | Vapour resistance coefficient | Water absorption coefficient | Water content at saturation | Source of values |
|---|---|---|---|---|---|---|---|
| | $\rho$ | $C_p$ | $\lambda$ | $\mu$ | $A_w$ | $W_{sat}$ | |
| | $(kg.m^{-3})$ | $(J.kg^{-1}.K^{-1})$ | $(W.m^{-1}.K^{-1})$ | (–) | $(kg.m^{-2}.s^{-0.5})$ | $(kg.m^{-3})$ | |
| Brick | 1616 | 800 | 0.49 | 9 | 0.28 | 388 | [62] |
| Calcium silicate | 186.8 | 1100 | 0.059 | 3.64 | 0.77 | 916.4 | Delphin database |
| Composite foil | 1276 | 1000 | 0.23 | 94384.5 | 0 | 113 | Delphin database |
| Concrete | 2104.2 | 1000 | 2.1 | 76.12 | 0.01 | 219.9 | Delphin database |
| Expanded polystyrene | 23 | 1500 | 0.036 | 96 | 0 | 920 | Delphin database |
| Glue mortar | 1409.9 | 1059 | 0.6 | 22.89 | 0 | 340 | Delphin database |
| Gypsum board | 850 | 850 | 0.2 | 10 | 0.28 | 551 | Delphin database |
| Hemp and lime insulation | 440 | 1000 | 0.07 | 6.5 | 0.2 | 789 | [62] |
| Lime plaster | 1249.9 | 999 | 0.57 | 12.14 | 0.13 | 452.2 | Delphin database |
| Mineral fine plaster | 586.3 | 1198 | 0.134 | 12.64 | 0.07 | 360 | Delphin database |
| Mineral wool | 37 | 840 | 0.04 | 1 | 0 | 900 | Delphin database |
| Old brick | 1715.2 | 920 | 0.543 | 22.17 | 0.14 | 322.1 | Delphin database |
| Perforated composite foil | 1276 | 1000 | 0.23 | 600 | 0 | 113 | Delphin database |
| Phenolic foam | 35.5 | 1470 | 0.02 | 113.73 | 0.01 | 501.2 | Delphin database |
| Plasterboard | 1043.4 | 1047 | 0.261 | 11.28 | 0.37 | 356 | Delphin database |
| Raw earth | 1730 | 648 | 0.6 | 9.83 | 0.39 | 345 | [61] |
| Vapour retarder | 1000 | 1400 | 0.15 | 1533 | 0 | 9 | Delphin database |
| Wood fibre boad | 150 | 2000 | 0.042 | 3 | 0.07 | 600 | Delphin database |

**Table 6**
Threshold values for the gap between the proposed tool and Delphin.

| | T (°C) | $P_{vap}$ (Pa) | w (kg .$m^{-3}$) |
|---|---|---|---|
| Type of error | *absolute* | *relative* | *relative* |
| Threshold value | 1 | 5% | 10% |

permeable, hygroscopic, and capillary active materials, which are characteristic of traditional and bio-based materials (Fig. 7).

Seven of the nineteen simulations gave partly unsatisfactory results (Fig. 7), which highlights the limitations of the numerical scheme associated with a coarse mesh. The results were less satisfactory for contemporary solutions, such as concrete – alone or insulated from the outside or inside. Also, the proposed method did not always effectively simulate walls composed of more than four layers of materials, for example wall n°13. The number of nodes was not sufficient to describe the strong variations induced by material changes.

In a second proposal, the mesh was refined. This version 2 of the mesh was characterised by a first mesh of 2.5 mm with a stretch factor of 1.7. Thus, the walls had between 9 and 16 nodes depending on their thickness.

With this refined mesh, the results became satisfactory for walls made of concrete. On the other hand, the results remained partly unsatisfactory for walls 13 and 14, which were composed of five and four layers of material, respectively (Fig. 8).

A third version of the mesh was tested with the aim of obtaining satisfactory results for all walls, including those with four or more layers of material. In this version, the mesh was further refined and was characterised by a first mesh size of 1 mm and a stretch factor of 1.5. Thus, the walls had a spatial discretisation between 15 and 23 nodes depending on their thickness. Finally, the results obtained (Fig. 9) show that the mesh thus refined made it possible to obtain satisfactory results for all the simulations.

### 4.4. Example of detailed results

This sub-section presents extracts of results, for the brick/hemp wall (n°1) (Fig. 10), in the climate of Cahors. The study period is five days, from 22nd to 27th November 2016. A rain event took place during the night of 22–23 November, which wetted the wall. During the following days, the drying of the wall can be observed. Fig. 11 describes the main variables used to calculate exterior boundary conditions. The proposed numerical scheme associated with the three mesh versions is compared with the Delphin reference tool.

Fig. 12 shows very satisfactory results for the temporal evolution of temperature and vapour pressure at the external surface for the three mesh versions, although a slight deviation is sometimes observed for the coarsest mesh size (version 1). This error can be explained by the larger size of the first mesh for this mesh version.

The three versions of the mesh are able to represent the spatial

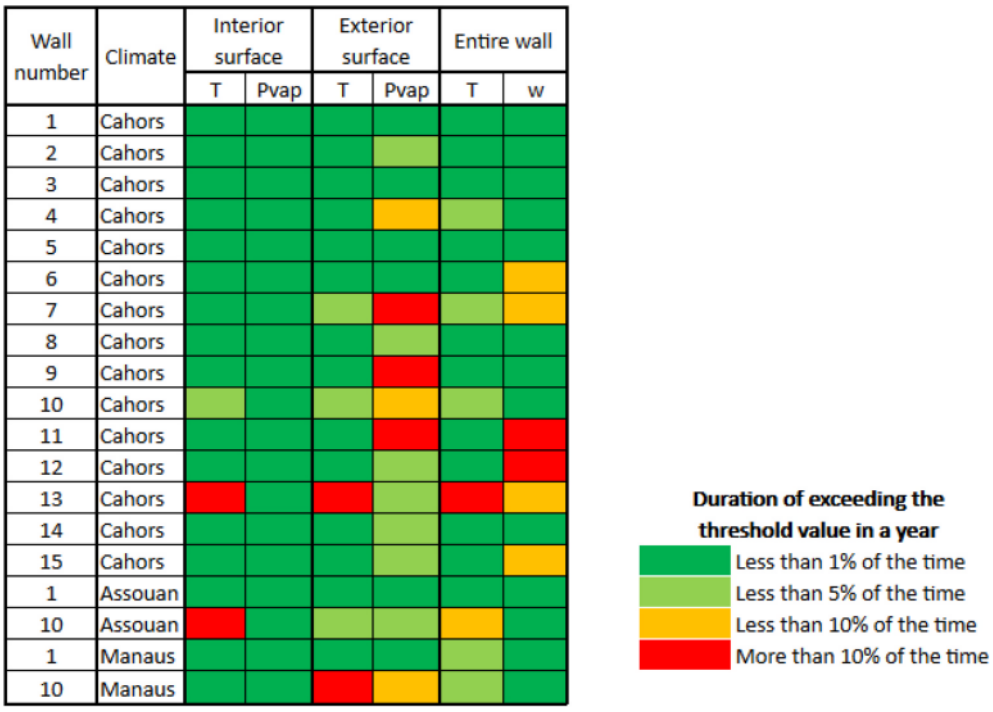


**Fig. 7.** Time during which the threshold value was exceeded in a year for each simulation with mesh version 1.

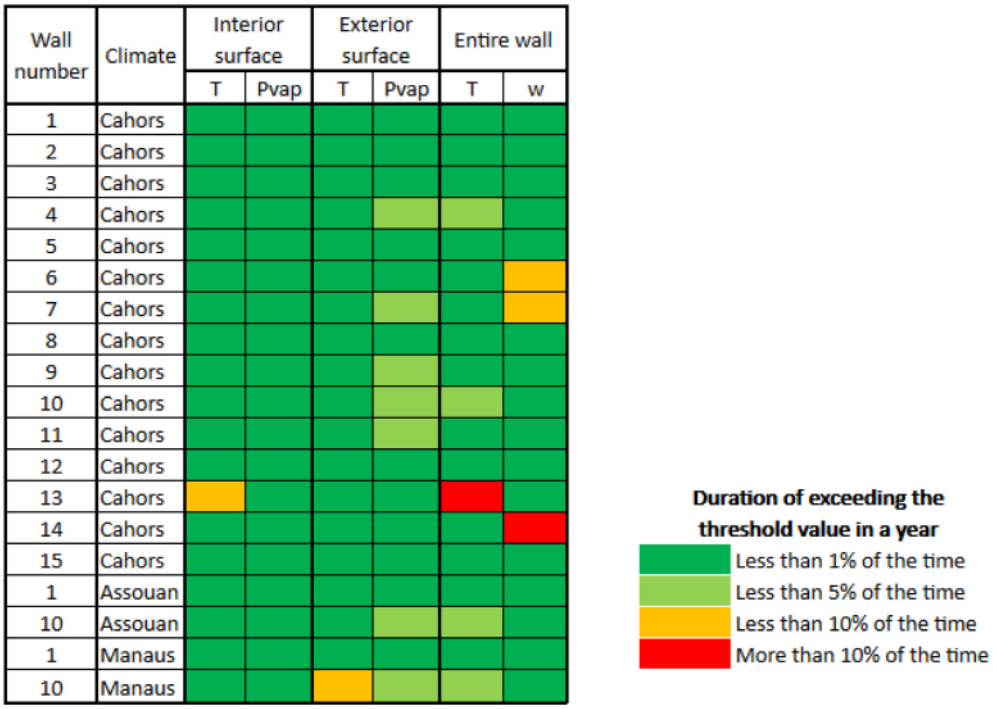


**Fig. 8.** Time during which the threshold value was exceeded in a year for each simulation with mesh version 2.

evolution of the temperature and water content in the wall very well and even version 1, with a very coarse mesh, can represent the profile in the wall in a very satisfactory way, during wetting phase (Fig. 13) and drying phase (Fig. 14).

As the aim was to evaluate the impact of hygrothermal transfers on the urban canyon balance, a complementary observation was carried out to evaluate the heat and mass fluxes exchanged with the environment at the outdoor surface. Fig. 15 shows the results for these fluxes, which are also satisfactory.

The numerical validation provides quite satisfactory results, including during the drying and wetting phases. A similar study was carried out for a warm and sunny period. The results are presented in the appendix. Several versions of the mesh have been compared. The version used must be chosen according to the type of material simulated, the number of material layers and the level of accuracy required.

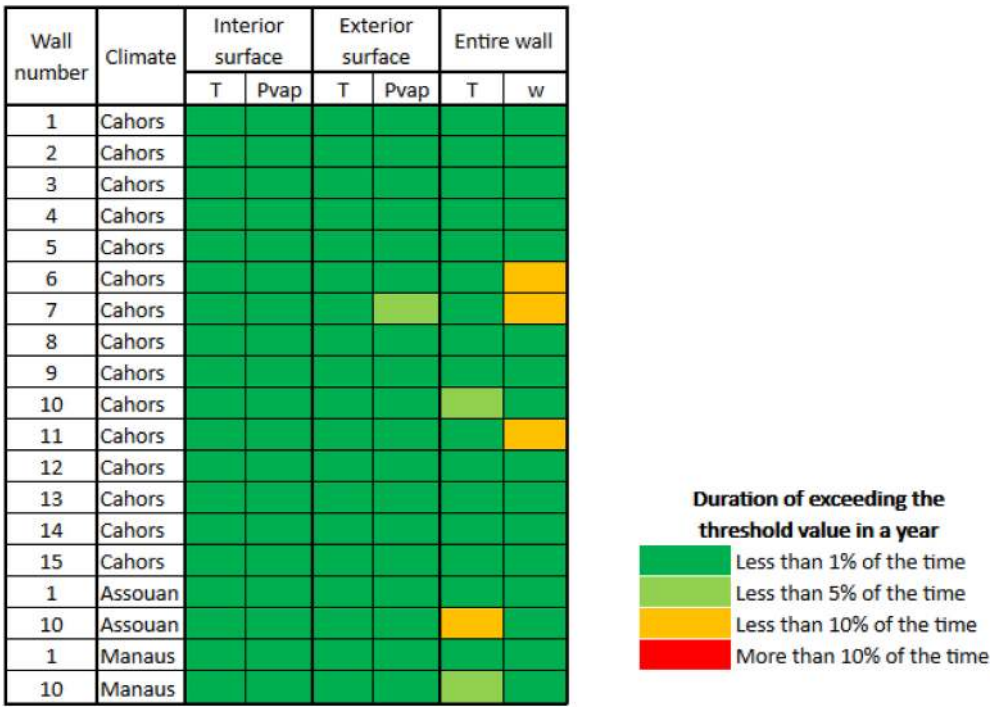


**Fig. 9.** Time during which the threshold value was exceeded in a year for each simulation with mesh version 3.

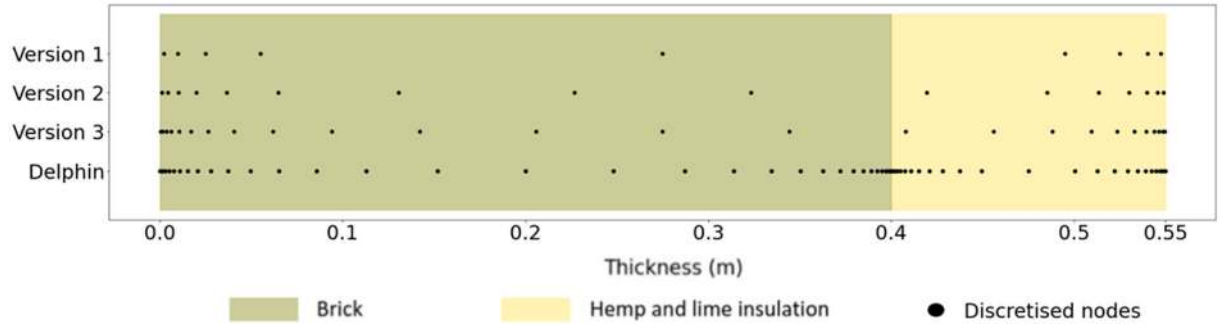


**Fig. 10.** The studied mesh versions applied to the brick wall insulated with hemp-lime.

## 5. Discussion

The results are considered acceptable for the urban scale, because the same level of accuracy is not expected as for a wall scale model: in an urban model, an entire neighbourhood is represented by a typical street, which means that, in an urban area, only one building, with typical characteristics of the studied area, is represented. Thus, walls are not modelled individually but by a single composition for the neighbourhood. Considering the approximations made on the composition of the walls and the characteristics of the materials, very accurate results cannot be expected.

This new numerical scheme is fully designed to be easily integrated into an urban model. For this purpose, the numerical scheme has been simplified and the spatial and temporal resolution scales have been adapted compared to a classical resolution scheme for coupled heat and mass transfers.

Many models, like Delphin, use implicit schemes that require sub-iterations at each time step until convergence is reached. The proposed scheme does not have this constraint as it uses an implicit/explicit scheme. Thus, only one iteration per time step ensures numerical stability, which is more consistent with the numerical scheme of an urban climate model like TEB.

In addition, a new, decoupled numerical solution approach is implemented. It has the advantage of completely separating the resolution of the heat equation from that of the mass conservation equation. This adaptation preserves the structure of the existing urban model code, while maintaining a satisfactory level of accuracy on the coupled transfers.

Regarding the time resolution scales, it was decided not to integrate a fully variable time step that would be adapted to each time step according to convergence. The method used is rather a fixed time step corresponding to that of a typical urban climate model (5 min), which is reduced, at moments critical for numerical stability, to a sub-time step of fixed duration (10 s). The integration of only two different time steps

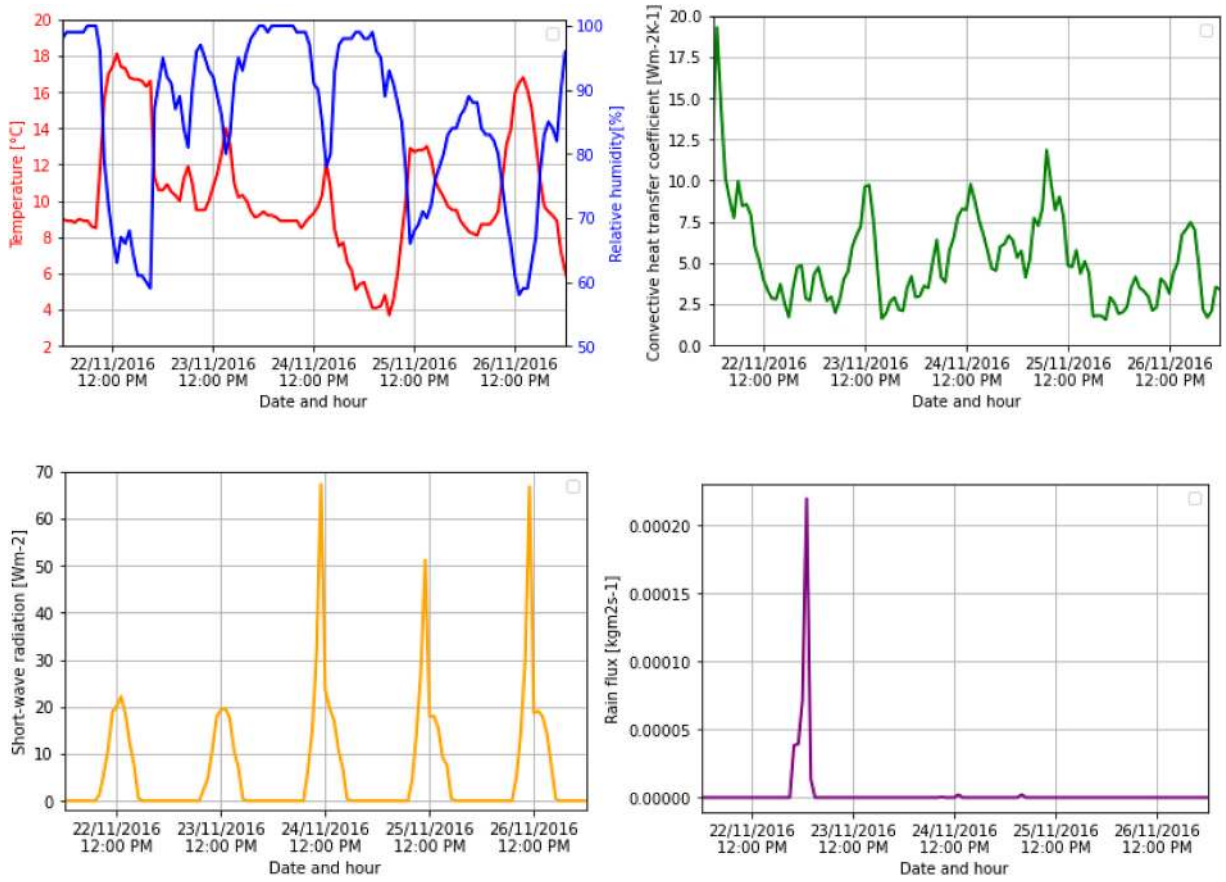


**Fig. 11.** Main variables used to calculate the exterior boundary conditions: outdoor temperature and relative humidity (top left), convective heat transfer coefficient (top right), solar radiation incident on the wall (bottom left) and rain flux incident on the wall (bottom right).

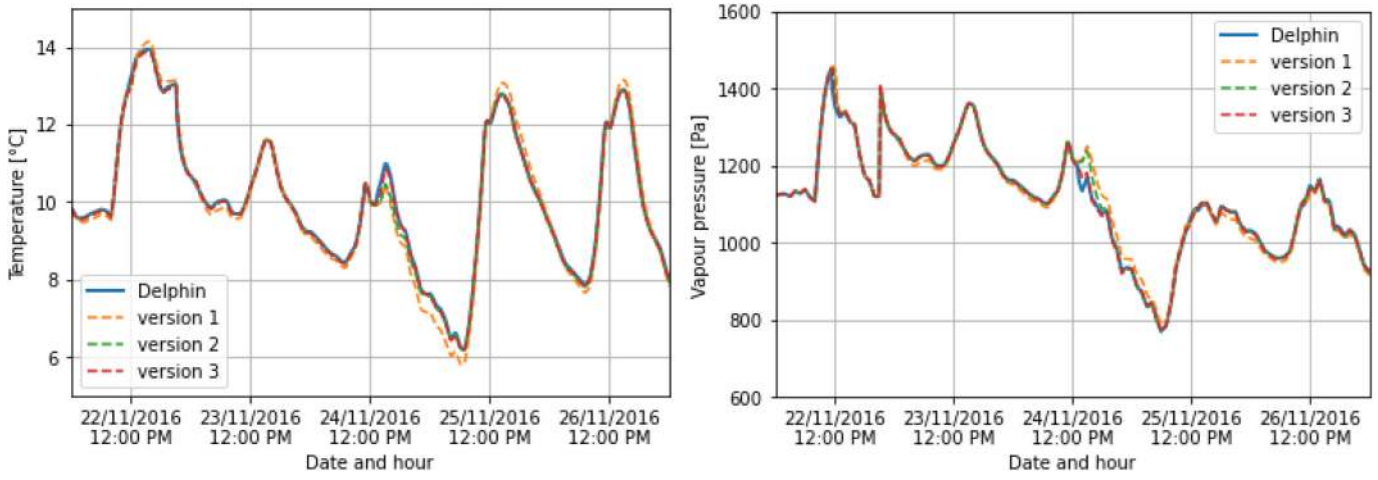


**Fig. 12.** Temporal evolution of temperature (left) and vapour pressure (right) at the exterior surface from 22nd to 27th November 2016 in Cahors.

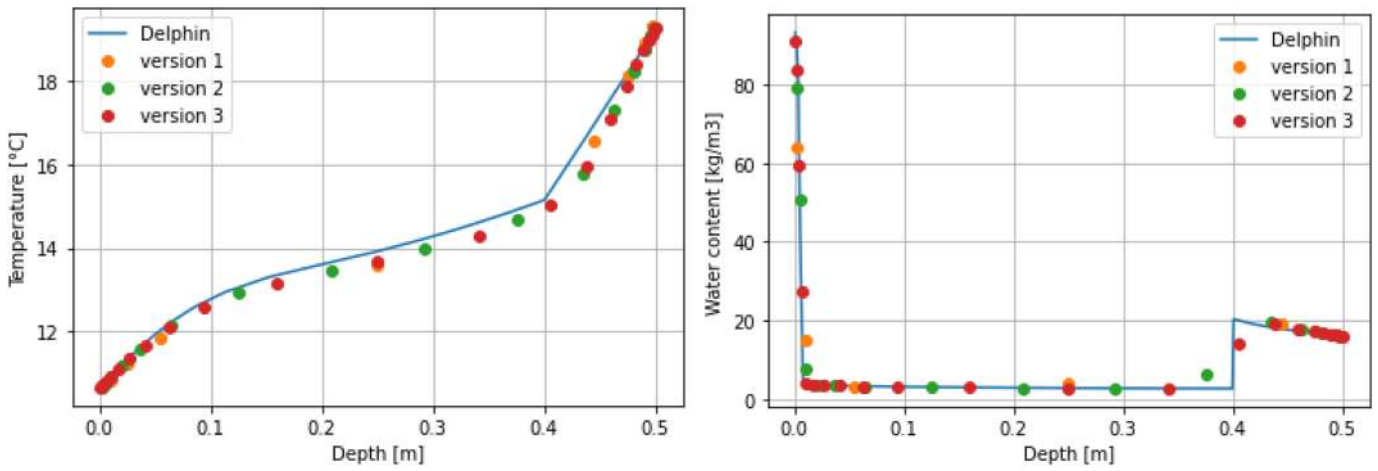


**Fig. 13.** Profile of temperature (left) and water content (right) in the wall on 23rd November 2016 at midnight in Cahors.

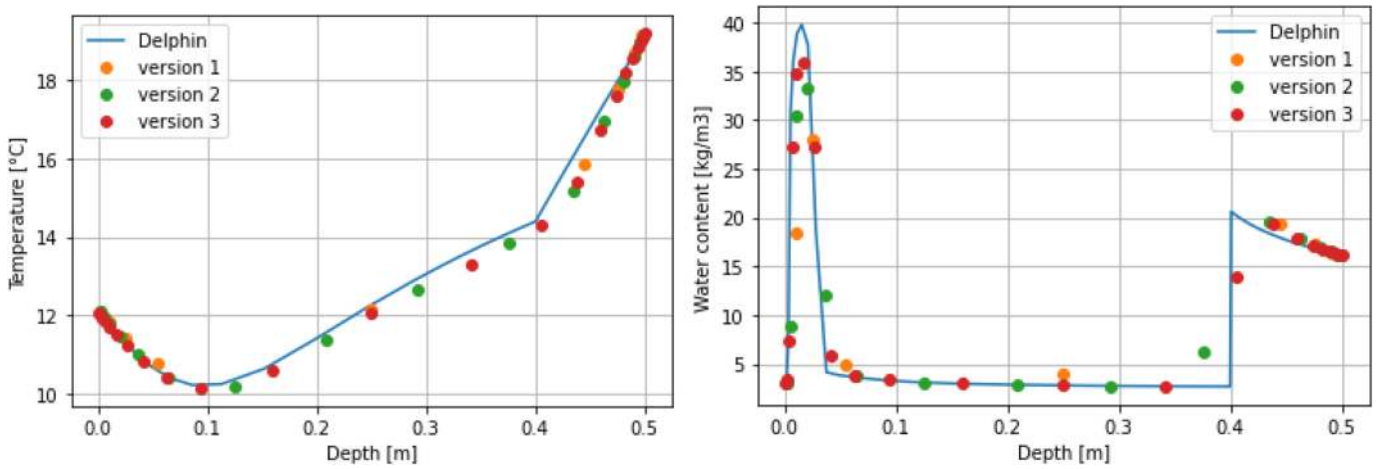


**Fig. 14.** Profile of temperature (left) and water content (right) in the wall on 25th November 2016 at noon in Cahors.

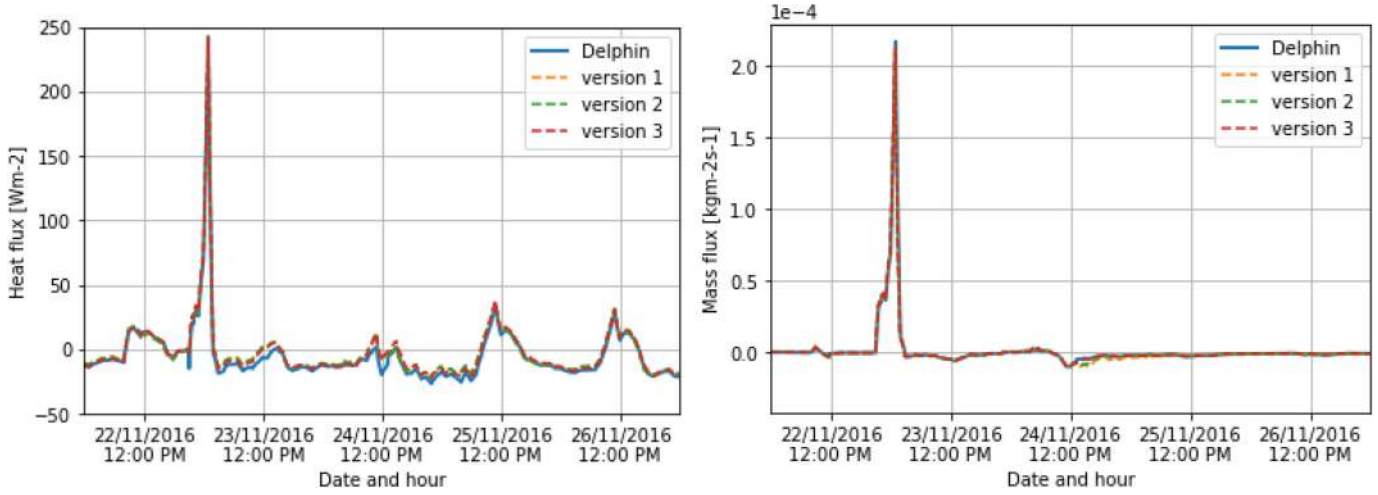


**Fig. 15.** Temporal evolution of heat flux (left) and mass flux (right) at the exterior surface from 22nd to 27th November 2016 in Cahors.

optimises the computation time and ensures numerical stability, while integrating well with a complex model simulating many physical processes. This simple method avoids any further complication of the urban model.

The last originality is the implementation of a rather coarse mesh, which is only refined at the interior and exterior surfaces and not at the interfaces of the materials. This type of mesh makes it possible to concentrate the calculation efforts on the zones of interest, which are the surfaces. At the urban scale, the elements of interest are the flux exchanged with the urban canyon or the interior environment, and not the conditions inside the wall. This meshing technique could be optimised by incorporating a method to adapt the mesh at each time step according to the location of the strongest temperature and water content gradients.

Finally, this paper has proposed a suitable numerical scheme for the simulation of coupled mass and heat transfers at urban scale. Its future integration in an urban model will enable energy/climate simulations to be performed including coupled transfers through walls over large spatial areas and long durations. The results thus obtained will complete the literature concerning the share of walls in the urban water balance and also the impact of moisture transfers in walls on conditions in the urban canyon. These results will have the advantage of being obtained for real weather conditions and by performing energy simulations in parallel to obtain the conditions inside the buildings. Thus, the integration in an urban climate model will enable the effect of considering this phenomenon to be evaluated both on the energy consumption of the HVAC equipment and on the indoor and outdoor comfort, by studying the moisture buffering capacity of walls and the potential of cooling by evaporation. These studies could be carried out on different wall compositions in order to compare them.

## 6. Conclusion

The issue of this article was to develop a suitable solution method for the integration of coupled mass and heat transfers in walls into a model at the urban scale. Several barriers have been raised, in particular concerning the scales of spatiotemporal resolution and the numerical schemes, which are different at the urban scale and at the wall scale. Compromises have been found to ensure reasonable computational cost and satisfactory quality of results.

Thus, the proposed solution method consists of an IMEX (implicit/explicit) scheme combined with a decoupled numerical resolution approach. The time step has been fixed at 5 min with a decrease to 10 s in the moments critical for numerical stability, which are identified by five tests.

Numerical validation of the method was performed using a model intercomparison method on several cases. It was based on the Delphin reference model and included fifteen wall compositions and three climates. Three mesh versions were compared, differing in the number of nodes, which ranged from 5 to 23.

The results show that a mesh size of less than nine nodes can be sufficient to simulate walls made of permeable materials. A larger number of nodes (about fifteen) is required to obtain satisfactory results for concrete walls with or without other materials. An even finer mesh size (about twenty nodes) is required to simulate walls with four or more layers of materials.

A detailed example has been presented. It concerns the simulation of an old brick wall insulated with hemp lime in the climate of Cahors. The temporal evolution at the surface level was studied for the following variables: temperature, vapour pressure, heat flux and mass flux. The three mesh versions obtained very satisfactory results despite a slight difference in temporal evolution for the coarsest mesh. In addition, the three meshes studied were able to effectively describe temperature and water content profiles in the wall. Thus, the results obtained agree with the level of accuracy expected for simulating coupled transfers in urban scale models.

The next step will be the integration of the model and the proposed method into the urban climate model TEB. Energy-climate simulations on an urban scale will be carried out and will be able to enrich the literature concerning not only the share of hydric transfers in the urban balance but also their impacts on energy consumption as well as on indoor and outdoor comfort. Our next objective is more specifically to simulate historic city centres, over long periods, in order to compare several renovation scenarios, and then to formulate recommendations on the most suitable renovation strategies with regard to energy and microclimate issues.

## CRediT authorship contribution statement

**Margot Ruiz:** Methodology, Investigation, Formal analysis, Writing – original draft. **Valéry Masson:** Methodology, Supervision, Writing – review & editing. **Marion Bonhomme:** Methodology, Supervision, Writing – review & editing. **Stéphane Ginestet:** Methodology, Supervision, Writing – review & editing.

## Declaration of competing interest

The authors declare that they have no known competing financial interests or personal relationships that could have appeared to influence the work reported in this paper.

## Data availability

No data was used for the research described in the article.

## Acknowledgements

This work was funded by the University of Toulouse and the Occitanie region, France. The authors wish to thank the city of Cahors for supporting the work.

## Appendix

This appendix presents an extract of the results of the comparison between the Delphin reference tool and the developed method associated with the three mesh versions. This part focuses on the brick/hemp wall (n°1) in the climate of Cahors. The study period is five days, from 4th to 9th July 2016. It covers a warm and sunny period, without rainfall. Figure A.1 describes the main variables used for the calculation of the outdoor boundary conditions.

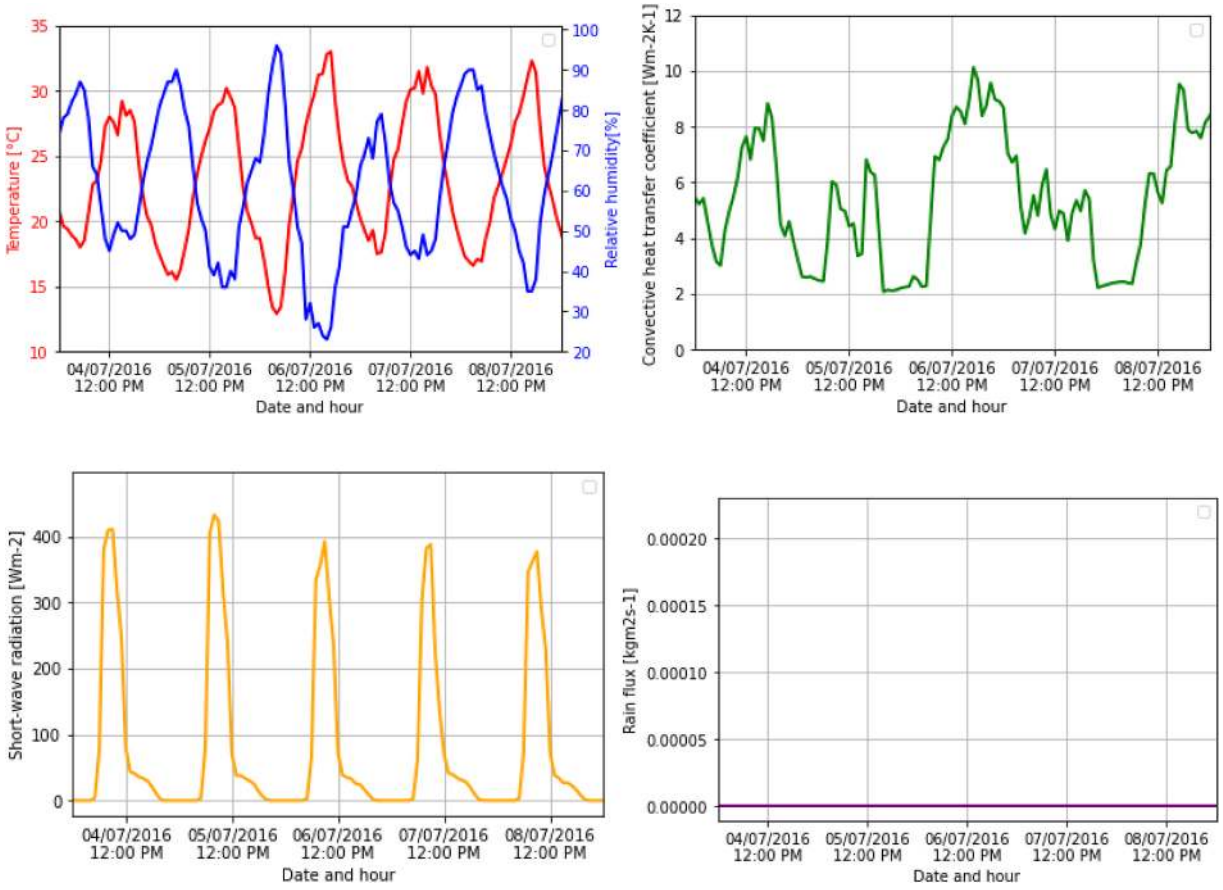


**Fig. A.1.** Main variables used to calculate the exterior boundary conditions: outdoor temperature and relative humidity (top left), convective heat transfer coefficient (top right), solar radiation incident on the wall (bottom left) and rain flux incident on the wall (bottom right)

Figure A.2 shows very satisfactory results for the temporal evolution of temperature and vapour pressure at the external surface for the three mesh versions.

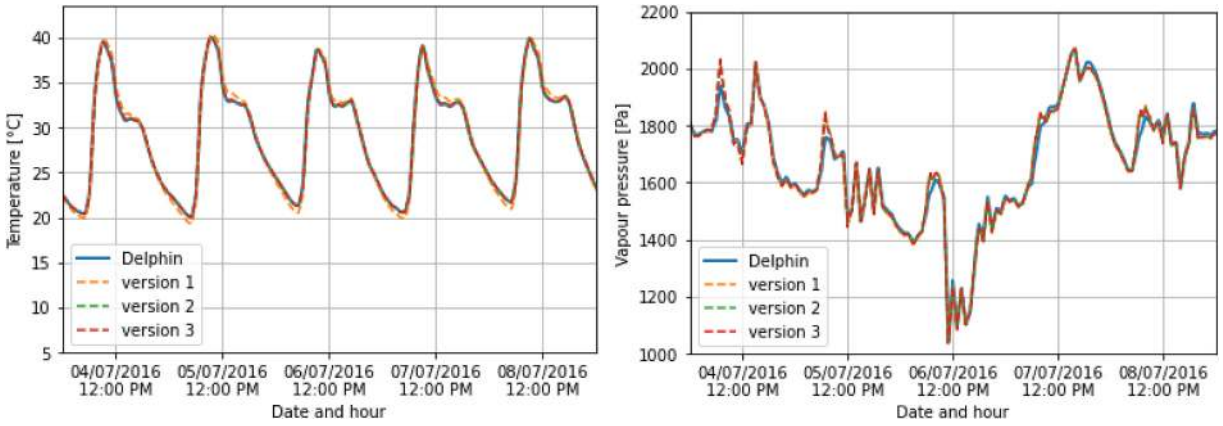


**Fig. A.2.** Temporal evolution of temperature (left) and vapour pressure (right) at the exterior surface from 4th to 9th July 2016 in Cahors

The objective of this appendix is to verify the validity of the model on sunny days. The behaviour of the temperature and water content in the wall was studied at the time of day when the shortwave radiation incident on the façade is maximum. According to Figure A.3, the three versions of the mesh are able to represent the spatial evolution of the temperature and water content in the wall in a very satisfactory way.

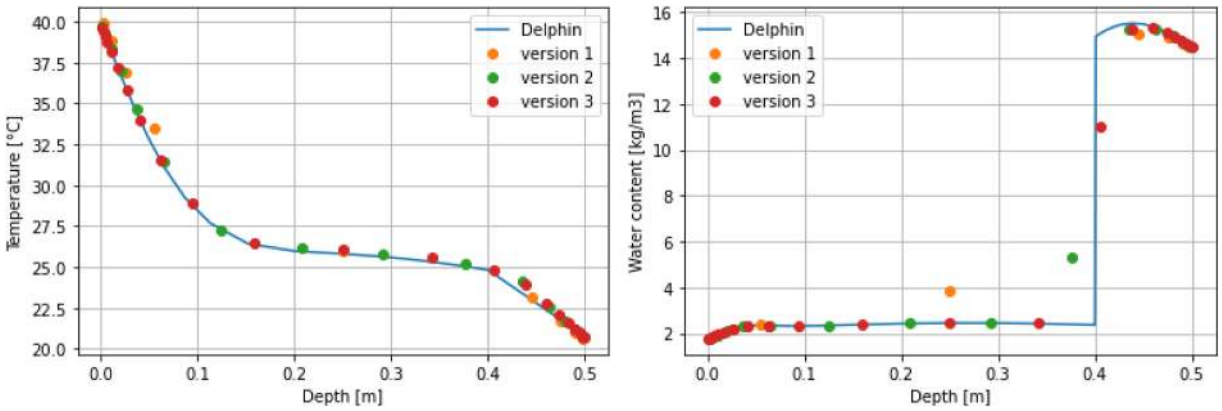


**Fig. A.3.** Profile of temperature (left) and water content (right) in the wall on 8th July 2016 at 9:30AM in Cahors

Figure A.4 shows the results obtained for the heat and mass flux at the exterior surface. They are satisfactory for all three versions, although a slight difference in amplitude is observed on the negative mass flux peaks. It is important to note that the mass flux exchanged is low.

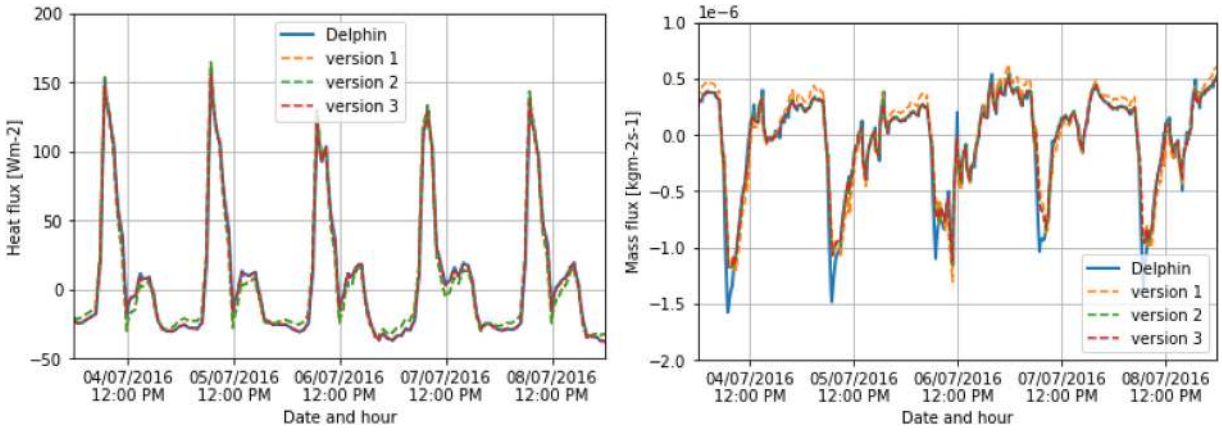


**Fig. A.4.** Temporal evolution of heat flux (left) and mass flux (right) at the exterior surface from 4th to 8th July 2016 in Cahors

The results obtained are rather satisfactory for the three mesh versions. Therefore, the method is also suitable for simulating the hygrothermal behaviour of walls under summer conditions.

## References


[1] Z. Wang, J. Song, P.W. Chan, Y. Li, The urban moisture island phenomenon and its mechanisms in a high-rise high-density city, Int. J. Climatol. (2020), https://doi.org/10.1002/joc.6672.

[2] S. Saneinejad, P. Moonen, J. Carmeliet, Coupled CFD, radiation and porous media model for evaluating the micro-climate in an urban environment, J. Wind Eng. Ind. Aerod. 128 (2014) 1–11, https://doi.org/10.1016/j.jweia.2014.02.005.

[3] A. Kubilay, D. Derome, J. Carmeliet, Coupling of physical phenomena in urban microclimate: a model integrating air flow, wind-driven rain, radiation and transport in building materials, Urban Clim. 24 (2018) 398–418, https://doi.org/10.1016/j.uclim.2017.04.012.

[4] S. Saneinejad, P. Moonen, T. Defraeye, D. Derome, J. Carmeliet, Coupled CFD, radiation and porous media transport model for evaluating evaporative cooling in an urban environment, J. Wind Eng. Ind. Aerod. 104–106 (2012) 455–463, https://doi.org/10.1016/j.jweia.2012.02.006.

[5] J. Yang, K.W. Tham, S.E. Lee, M. Santamouris, C. Sekhar, D.K.W. Cheong, Anthropogenic heat reduction through retrofitting strategies of campus buildings, Energy Build. 152 (2017) 813–822, https://doi.org/10.1016/j.enbuild.2016.11.051.

[6] N. Mendes, F.C. Winkelmann, R. Lamberts, P.C. Philippi, Moisture effects on conduction loads, Energy Build. 35 (2003) 631–644, https://doi.org/10.1016/S0378-7788(02)00171-8.

[7] R.M. Barbosa, N. Mendes, Combined simulation of central HVAC systems with a whole-building hygrothermal model, Energy Build. 40 (2008) 276–288, https://doi.org/10.1016/j.enbuild.2007.02.022.

[8] X. Liu, Y. Chen, H. Ge, P. Fazio, G. Chen, Numerical investigation for thermal performance of exterior walls of residential buildings with moisture transfer in hot summer and cold winter zone of China, Energy Build. 93 (2015) 259–268, https://doi.org/10.1016/j.enbuild.2015.02.016.

[9] X. Zhou, J. Carmeliet, M. Sulzer, D. Derome, Energy-efficient mitigation measures for improving indoor thermal comfort during heat waves, Appl. Energy 278 (2020), 115620, https://doi.org/10.1016/j.apenergy.2020.115620.

[10] M. Woloszyn, T. Kalamees, M. Olivier Abadie, M. Steeman, A. Sasic Kalagasidis, The effect of combining a relative-humidity-sensitive ventilation system with the moisture-buffering capacity of materials on indoor climate and energy efficiency of buildings, Build. Environ. 44 (2009) 515–524, https://doi.org/10.1016/j.buildenv.2008.04.017.

[11] M. Lawrence, A. Shea, P. Walker, P. De Wilde, Hygrothermal performance of bio-based insulation materials, Proc. Inst. Civ. Eng. - Constr. Mater. 166 (2013) 257–263, https://doi.org/10.1680/coma.12.00031.

[12] H. Ge, X. Yang, P. Fazio, J. Rao, Influence of moisture load profiles on moisture buffering potential and moisture residuals of three groups of hygroscopic materials, Build. Environ. 81 (2014) 162–171, https://doi.org/10.1016/j.buildenv.2014.06.021.

[13] L. Fang, G. Clausen, P.O. Fanger, Impact of temperature and humidity on the perception of indoor air quality, Indoor Air 8 (1998) 80–90, https://doi.org/10.1111/j.1600-0668.1998.t01-2-00003.x.

[14] S. Atthajariyakul, T. Leephakpreeda, Real-time Determination of Optimal Indoor-Air Condition for Thermal Comfort, Air Quality and Efficient Energy Usage, Energy Build., 2004, pp. 720–733.

[15] C. Maalouf, A.D.T. Le, S.B. Umurigirwa, M. Lachi, O. Douzane, Study of hygrothermal behaviour of a hemp concrete building envelope under summer conditions in France, Energy Build. 77 (2014) 48–57, https://doi.org/10.1016/j.enbuild.2014.03.040.

[16] O.F. Osanyintola, C.J. Simonson, Moisture buffering capacity of hygroscopic building materials: experimental facilities and energy impact, Energy Build. 38 (2006) 1270–1282, https://doi.org/10.1016/j.enbuild.2006.03.026.

[17] M. Zhang, M. Qin, C. Rode, Z. Chen, Moisture buffering phenomenon and its impact on building energy consumption, Appl. Therm. Eng. 124 (2017) 337–345, https://doi.org/10.1016/j.applthermaleng.2017.05.173.

[18] H.M. Künzel, Simultaneous Heat and Moisture Transport in Building Components: One- and Two-Dimensional Calculation Using Simple Parameters, IRB Verlag, Stuttgart, 1995.
[19] M. Krus, Moisture Transport and Storage Coefficients of Porous Mineral Building Materials Theoretical Principles and New Test Methods, Fraunhofer-IRB-Verl., Stuttgart, 1996.
[20] J.R. Philip, D.A. De Vries, Moisture movement in porous materials under temperature gradients, Trans. Am. Geophys. Union 38 (1957) 222, https://doi.org/10.1029/TR038i002p00222.
[21] A.V. Luikov, Systems of differential equations of heat and mass transfer in capillary-porous bodies (review), Int. J. Heat Mass Tran. 18 (1975) 1–14, https://doi.org/10.1016/0017-9310(75)90002-2.
[22] J. Delgado, N. Ramos, E. Barreira, V. Freitas, A Critical Review of Hygrothermal Models Used in Porous Building Materials, vol. 13, J. Porous Media - J POROUS MEDIA, 2010, pp. 221–234, https://doi.org/10.1615/JPorMedia.v13.i3.30.
[23] A. Nicolai, Modeling and Numerical Simulation of Salt Transport and Phase Transitions in Unsaturated Porous Building Materials, 2007, https://doi.org/10.13140/RG.2.1.2016.2088.
[24] C. Rode Pedersen, Combined Heat and Moisture Transfer in Building Constructions, Danmarks Tekniske Hoejskole, Lyngby (Denmark), Lab. for Varmeisolering, 1990.
[25] A. Sasic Kalagasidis, T. Bednar, C.-E. Hagentoft, The evaluation of the interface moisture conductivity between control volumes. Comparison between linear, harmonic and integral averaging, in: 9th Int. Conf. Perform. Exter. Envel, . Whole Build., Clearwater Beach, Florida, 2004, 2004.
[26] J. Berger, S. Gasparin, D. Dutykh, N. Mendes, On the comparison of three numerical methods applied to building simulation: finite-differences, RC circuit approximation and a spectral method, Build. Simulat. 13 (2020) 1–18, https://doi.org/10.1007/s12273-019-0555-z.
[27] D. Costola, B.J.E. Blocken, J.L.M. Hensen, External Coupling between BES and HAM Programs for Whole Building Simulation, in: 11th Int. Build. Perform. Simul. Conf. 27-30 July 2009 Glasg. Scotl., International Building Performance Simulation Association (IBPSA), 2009, pp. 316–323.
[28] M. Woloszyn, C. Rode, Tools for performance simulation of heat, air and moisture conditions of whole buildings, Build. Simulat. 1 (2008) 5–24, https://doi.org/10.1007/s12273-008-8106-z.
[29] J. Yang, H. Fu, M. Qin, Evaluation of different thermal models in EnergyPlus for calculating moisture effects on building energy consumption in different climate conditions, Procedia Eng. 121 (2015) 1635–1641, https://doi.org/10.1016/j.proeng.2015.09.194.
[30] T. Kalamees, I.C.E. Ida, The Simulation Tool for Making the Whole Building Energy- and HAM Analysis, 2004.
[31] C. Rode, K. Grau, Whole building hygrothermal simulation model, Build. Eng. 109 (2003).
[32] A.E. Nakhi, ADAPTIVE CONSTRUCTION MODELLING WITHIN WHOLE BUILDING DYNAMIC SIMULATION, University of Strathclyde, 1995.
[33] F. Tariku, K. Kumaran, P. Fazio, Integrated analysis of whole building heat, air and moisture transfer, Int. J. Heat Mass Tran. 53 (2010) 3111–3120, https://doi.org/10.1016/j.ijheatmasstransfer.2010.03.016.
[34] B. Blocken, S. Roels, J. Carmeliet, A combined CFD–HAM approach for wind-driven rain on building facades, J. Wind Eng. Ind. Aerod. 95 (2007) 585–607, https://doi.org/10.1016/j.jweia.2006.12.001.
[35] C. Grimmond, M. Best, J. Barlow, A. Arnfield, J.-J. Baik, A. Baklanov, S.E. Belcher, M. Bruse, I. Calmet, P. Clark, A. Dandou, E. Erell, K. Fortuniak, R. Hamdi, M. Kanda, T. Kawai, H. Kondo, E. Krayenhoff, T. Williamson, Urban surface energy balance models: model characteristics and methodology for a comparison study, in: Meteorol. Air Qual. Models, Urban Areas, 2009, pp. 97–123, https://doi.org/10.1007/978-3-642-00298-4_11.
[36] V. Masson, A physically-based scheme for the urban energy budget in atmospheric models, Bound.-Layer Meteorol. 94 (2000) 357–397, https://doi.org/10.1023/A:1002463829265.
[37] H. Kusaka, H. Kondo, Y. Kikegawa, F. Kimura, A simple single-layer urban canopy model for atmospheric models: comparison with multi-layer and slab models, Bound, -Layer Meteorol 101 (2001) 329–358.
[38] A. Martilli, Numerical study of urban impact on boundary layer structure: sensitivity to wind speed, urban morphology, and rural soil moisture, J. Appl. Meteorol. 41 (2002) 1247–1266.
[39] T.R. Oke, The energetic basis of the urban heat island, Q. J. R. Meteorol. Soc. 108 (1982) 1–24, https://doi.org/10.1002/qj.49710845502.
[40] B. Bueno, G. Pigeon, L.K. Norford, K. Zibouche, C. Marchadier, Development and evaluation of a building energy model integrated in the TEB scheme, Geosci. Model Dev. (GMD) 5 (2012) 433–448, https://doi.org/10.5194/gmd-5-433-2012.
[41] J. Berger, S. Gasparin, N. Mendes, Accurate numerical simulation of moisture front in porous material, Build, Environ. Times 118 (2017) 211–224, https://doi.org/10.1016/j.buildenv.2017.03.016.
[42] J. Berger, N. Mendes, S. Guernouti, M. Woloszyn, F. Chinesta, Review of reduced order models for heat and moisture transfer in building physics with emphasis in PGD approaches, Arch. Comput. Methods Eng. 24 (2017) 655–667, https://doi.org/10.1007/s11831-016-9184-1.
[43] H. Janssen, B. Blocken, J. Carmeliet, Conservative modelling of the moisture and heat transfer in building components under atmospheric excitation, Int. J. Heat Mass Tran. 50 (2007) 1128–1140, https://doi.org/10.1016/j.ijheatmasstransfer.2006.06.048.
[44] H. Hens, Heat, Air and Moisture Transfer in Highly Insulated Building Envelopes (HAMTIE), FaberMaunsell Limited, 2002.
[45] J. Carmeliet, D.M.H. Wit, H. Janssen, Hysteresis and moisture buffering of wood, in: Proc. 7th Symp. Build. Phys. Nord, Ctries. Reyk., 2005, pp. 55–62.
[46] M. Libralato, A. De Angelis, O. Saro, M. Qin, C. Rode, Effects of considering moisture hysteresis on wood decay risk simulations of building envelopes, J. Build. Eng. 42 (2021), 102444, https://doi.org/10.1016/j.jobe.2021.102444.
[47] S. Vogelsang, H. Fechner, A. Nicolai, Delphin 6 Material File Specification, 2013.
[48] Q. Li, J. Rao, P. Fazio, Development of HAM tool for building envelope analysis, Build. Environ. 44 (2009) 1065–1073, https://doi.org/10.1016/j.buildenv.2008.07.017.
[49] H. Janssen, Simulation efficiency and accuracy of different moisture transfer potentials, J. Build. Perform. Simul. 7 (2014), https://doi.org/10.1080/19401493.2013.852246.
[50] S. Gasparin, Numerical Methods for Predicting Heat and Moisture Transfer through Porous Building Materials, PhD Thesis, Université Grenoble Alpes, Pontifícia universidade católica do Paraná, 2019.
[51] S. Gasparin, J. Berger, D. Dutykh, N. Mendes, An innovative method to determine optimum insulation thickness based on non-uniform adaptive moving grid, J. Braz. Soc. Mech. Sci. Eng. 41 (2019) 173, https://doi.org/10.1007/s40430-019-1670-6.
[52] S. Gasparin, J. Berger, N. Mendes, Stable explicit schemes for simulation of nonlinear moisture transfer in porous materials, J. Build. Perform. Simul. 11 (2017) 129–144, https://doi.org/10.1080/19401493.2017.1298669.
[53] W. Dong, Y. Chen, Y. Bao, A. Fang, A validation of dynamic hygrothermal model with coupled heat and moisture transfer in porous building materials and envelopes, J. Build. Eng. 32 (2020), 101484, https://doi.org/10.1016/j.jobe.2020.101484.
[54] L. Sontag, A. Nicolai, S. Vogelsang, Validierung der Solverimplementierung des hygrothermischen Simulationsprogramms Delphin, 2013.
[55] M. Mirsadeghi, D. Costola, B. Blocken, J.L. Hensen, Review of external convective heat transfer coefficient models in building energy simulation programs: implementation and uncertainty, Appl. Therm. Eng. 56 (2013) 134–151.
[56] J.A. Palyvos, A survey of wind convection coefficient correlations for building envelope energy systems' modeling, Appl. Therm. Eng. 28 (2008) 801–808, https://doi.org/10.1016/j.applthermaleng.2007.12.005.
[57] T. Defraeye, B. Blocken, J. Carmeliet, Convective heat transfer coefficients for exterior building surfaces: existing correlations and CFD modelling, Energy Convers. Manag. 52 (2011) 512–522, https://doi.org/10.1016/j.enconman.2010.07.026.
[58] Lawrence Berkeley Laboratory (LBL), DOE2.1E-053 Source Code, 1994.
[59] I.S.O. NF EN, Performance hygrothermique des bâtiments - Calcul et présentation des données climatiques - Partie 3 : calcul d'un indice de pluie battante pour surfaces verticales à partir de données horaires de vent et de pluie, 2009, 15927-3.
[60] S.A. Orr, H. Viles, Characterisation of building exposure to wind-driven rain in the UK and evaluation of current standards, J. Wind Eng. Ind. Aerod. 180 (2018) 88–97, https://doi.org/10.1016/j.jweia.2018.07.013.
[61] L. Soudani, A. Fabbri, J.-C. Morel, M. Woloszyn, P.-A. Chabriac, H. Wong, A.-C. Grillet, Assessment of the validity of some common assumptions in hygrothermal modeling of earth based materials, Energy Build. 116 (2016) 498–511, https://doi.org/10.1016/j.enbuild.2016.01.025.
[62] S. Claude, Étude expérimentale et numérique de solutions basées sur les éco-matériaux pour la rénovation thermique du patrimoine bâti urbain, PhD Thesis, INSA de Toulouse, 2018.
[63] J. Lu, V. Marincioni, S.A. Orr, H. Altamirano-Medina, Climate resilience of internally-insulated historic masonry assemblies: comparison of moisture risk under current and future climate scenarios, Minerals 11 (2021) 271, https://doi.org/10.3390/min11030271.